Eur. Phys. J. D **28**, 11–38 (2004)
DOI: 10.1140/epjd/e2003-00305-4

THE EUROPEAN PHYSICAL JOURNAL D

On the muon transfer from protium to neon

S.V. Romanov[a]

Institute of General and Nuclear Physics, Russian Research Centre "Kurchatov Institute", Moscow 123 182, Russia

Received 18 February 2003 / Received in final form 9 September 2003
Published online 2nd December 2003 –

Abstract. The rate of the muon transfer from the 1S-state of muonic protium to neon is calculated in the interval of collision energies from 10^{-4} eV to 15 eV. The basic idea of the present treatment is to describe the entrance channel of the transfer reaction at large interatomic separations as correctly as possible. Accordingly, the three-body Hamiltonian is written in the Jacobi coordinates of the entrance channel, and a problem of the muon motion in the field of two fixed Coulomb centers is formulated in these coordinates. Its eigenstates are used as a basis in which the three-body wavefunction is expanded. Finally, the radial functions describing the relative motion in the entrance and transfer channels satisfy a set of coupled ordinary differential equations. Its solution allows one to find diagonal S-matrix elements corresponding to the entrance channel and, as a result, to obtain the total transfer cross-section and the amplitude of the elastic scattering. In this approach the description of the entrance channel proves to be free of the well-known defects — incorrect dissociation limits and spurious long-range interactions. These defects are manifested only in the transfer channel. However, their effect seems to be not very significant because of large energies of the relative motion in this channel (a few keV). The calculation made here with four two-center σ-states taken into account reasonably reproduces the experimental transfer rate measured in liquid hydrogen-neon mixtures. The situation at room temperatures is worse: the theoretical value of the transfer rate exceeds the experimental one by a factor of two. However, the calculation clearly indicates the existence of a well pronounced minimum of the transfer rate at thermal energies. This result corresponds qualitatively to the experimental fact of a strong suppression of the muon transfer at room temperatures. At collision energies of 0.3–0.5 eV a resonant peak in the transfer rate is predicted. It is due to a quasi-steady state in the D-wave. The elastic scattering of muonic protium by neon is also treated. The effect of the electron screening in the entrance channel is studied in detail. It is found to be very significant right up to collision energies of 1–2 eV.

PACS. 34.70.+e Charge transfer – 34.50.-s Scattering of atoms and molecules – 36.10.-k Exotic atoms and molecules (containing mesons, muons, and other unusual particles)

1 Introduction

The 2S and 2P states of muonic protium μp are known to be separated by the energy interval of 0.2 eV [1]. Unlike the Lamb shift in the ordinary hydrogen atom, this splitting is mostly due to the vacuum polarization so the 2S state is energetically lower. About two percent of the energy splitting is contributed by proton finite-size effects. The leading finite-size correction is proportional to the mean-square charge radius of the proton $\langle r_p^2 \rangle$. In principle, a precise measurement of the 2S−2P splitting makes it possible to determine the proton radius $r_p = \sqrt{\langle r_p^2 \rangle}$ with a high accuracy. Of course, in this case the other significant contributions to the splitting should be properly taken into account [2].

An experiment on measuring the 2S−2P splitting is now in progress at the Paul Scherrer Institute (PSI, Switzerland) [3,4]. Its idea is to produce $\mu p(2S)$ atoms in hydrogen gas, to excite the electric dipole transition between the hyperfine $|2S_{1/2}; F = 1\rangle$ and $|2P_{3/2}; F = 2\rangle$ components[1] with light pulses generated by a tunable laser and to record subsequent 2 keV X-rays emitted in the 2P → 1S muon transition. The X-rays intensity as a function of the laser wavelength should have a peak corresponding to the resonant excitation of the $2S \to 2P_{3/2}$ transition indicated above. If the peak shape is well established, the transition energy may be precisely determined and the proton radius r_p may be extracted. According to [3,4], the accuracy of 0.1% in r_p can be achieved. This is much better than the present few percent accuracy. The use of this value of r_p will allow one to test quantum

[a] e-mail: roman@pretty.mbslab.kiae.ru

[1] F is the total angular momentum of μp.

electrodynamics calculations of the ordinary hydrogen atom at a considerably higher precision level.

1.1 The μp(2S) metastability

The laser experiment may be performed provided there is an appreciable fraction of metastable μp(2S) atoms with the lifetime of the order of 1 μs. The dominant disappearance mode of the μp(2S) atom isolated from external perturbations is the muon decay so its lifetime is about 2 μs in this case. In a gaseous H_2 target an additional quenching of the 2S state occurs in collisions of the muonic atom with hydrogen molecules. This may be schematically written as follows:

$$\mu p\,(2\mathrm{S}) + \mathrm{H}_2 \rightarrow \mu p\,(1\mathrm{S}) + \mathrm{H}_2 + \gamma. \qquad (1)$$

γ denotes a 2 keV photon, the molecule H_2 may be in different vibrational and rotational states before and after the collision. The mechanism of the reaction (1) and its rate depend drastically on the muon-atom kinetic energy. If it exceeds the 2S $\rightarrow$ 2P excitation threshold (0.2 eV in the center-of-mass frame or 0.31 eV in the laboratory frame in which the hydrogen molecule is assumed to be initially in rest), the 2P state is excited during the collision and the photon is then emitted in the 2P $\rightarrow$ 1S muon transition. At the laboratory-frame kinetic energy $E_{\mathrm{lab}} \sim 1$ eV the collision time is shorter than the 2P state lifetime by three orders of magnitude so the radiation may be treated to occur after the collision. Within this approximation the cross-section σ_q of the reaction (1) was estimated in [5–7] by considering the quenching of μp(2S) in collisions with hydrogen atoms. It was found that σ_q increased with E_{lab} from zero at the threshold to 10^{-16} cm^2 at $E_{\mathrm{lab}} = 1{-}2$ eV [2]. Because of such large values of the cross-section the reaction (1) becomes the dominant disappearance mode of the 2S state at H_2 pressures of a few mbar. For example, at 1 mbar the lifetime of μp(2S) with $E_{\mathrm{lab}} > 1$ eV is less than 0.2 μs.

If the muon-atom kinetic energy is below the 2S $\rightarrow$ 2P excitation threshold, the situation changes qualitatively. In this case the radiative muon transition occurs during the collision due to the Stark mixing of the 2S and 2P states induced by the electric field of the hydrogen molecule. Because of the smallness of the collision time compared to the 2P state lifetime, the cross-section of the reaction (1) becomes considerably less than that found in the above-threshold energy region. The corresponding calculations were made in [8,9] for μp(2S) collisions with hydrogen atoms. The quenching cross-section σ_q was obtained to be of the order of $10^{-18}{-}10^{-19}$ cm^2. Accordingly, typical rates of the reaction (1) are $10^3{-}10^4$ s^{-1} at a few mbar of H_2, so the collisional quenching is insignificant in this case and the muon-atom 2S state is metastable with the lifetime about 2 μs.

The fraction of the metastable μp(2S) atoms with the kinetic energies below the 2S $\rightarrow$ 2P excitation threshold (0.31 eV) is seen to relate to the laser experiment. This fraction is determined by both the initial energy distribution of μp(2S) atoms after their formation and the kinetics of their subsequent moderation in hydrogen. Concerning the initial energy distribution, it was experimentally studied for μp(1S) atoms only [10]. In order to increase the amount of muonic atoms with energies less than 1$-$2 eV, the experiment was performed at low H_2 pressures lying between 0.063 and 64 mbar. It is expected that at such small densities the energy distribution is nearly the same for the muonic atoms in the 1S and 2S states. It was thus found that at a few mbar of H_2 about 10% of μp(2S) atoms had subthreshold initial energies (below 0.31 eV). These muonic atoms are metastable from the beginning. Moreover, about 20% of the muonic atoms has initial energies between 0.31 and 1 eV. A part of such atoms remains unquenched in slowing down to 0.31 eV. This part was estimated in [6,7] where the transport and differential cross-sections of the elastic scattering of μp(2S) by H atoms were calculated and the migration kinetics of muonic atoms in hydrogen was considered. The part of the unquenched μp(2S) with the initial kinetic energy of 1 eV was obtained to be about 50% [3]. So, the amount of the muonic atoms in the 2S state which have the initial energies between 0.31 and 1 eV and remain unquenched in slowing down to the the 2S $\rightarrow$ 2P excitation threshold is, at least, 10%. In the sum with 10% of the initially subthreshold atoms this gives about 20% for the metastable μp(2S) fraction. Taking into account that the 2S state population found from X-ray measurements at a few mbar of H_2 is around 4% per one muon stop [11], the yield of the metastable μp(2S) atoms is obtained to be about 1% per one μp atom initially formed [3].

1.2 Searching for metastable μp(2S) atoms

The above-presented estimation of the yield of the metastable μp(2S) atoms is based on a number of indirect data. More direct measurements of the 2S state metastability were also performed at PSI [3,12]. The idea consisted in using the reaction of the muon transfer from the 2S state of muonic protium μp to neon [13]:

$$\mu p\,(2\mathrm{S}) + \mathrm{Ne} \rightarrow \mu\mathrm{Ne}^* + p. \qquad (2)$$

The final μNe* atom is formed in an excited state, the subsequent decay of which is accompanied by the emission of delayed K-series X-rays with energies around 200 keV. The muon transfer occurs also from the 1S state of μp:

$$\mu p\,(1\mathrm{S}) + \mathrm{Ne} \rightarrow \mu\mathrm{Ne}^* + p. \qquad (3)$$

[2] The behaviour of σ_q near the 2S $\rightarrow$ 2P excitation threshold needs a more refined treatment taking into account the finite 2P state width. Actually, σ_q does not equal to zero at the threshold, but it drops rapidly as E_{lab} migrates into the subthreshold region [5]. Of course, the fine and hyperfine structure should be also taken into account in such a treatment.

[3] The part of the unquenched muonic atoms falls rapidly with increasing the initial kinetic energy. For example, it is 4% at the initial energy of 5 eV [7].

The X-rays emitted by muonic neon formed in this process are a background for the reaction (2). A favourable circumstance which caused the choice of neon for the search for $\mu p(2S)$ atoms is that the reaction (3) is strongly suppressed. Its rate was measured in gaseous hydrogen-neon mixtures at room temperatures, the total pressure of 15 and 38 bar and neon concentrations of 0.7−2.0% [14]. The result obtained is:

$$\lambda_t^{\mu p}(1S) = (0.0849 \pm 0.0018) \times 10^{11}\ \mathrm{s}^{-1}. \quad (4)$$

This value is traditionally reduced to the atomic density of liquid hydrogen (the number of protons in cm^3):

$$N_{\mathrm{H}} = 4.25 \times 10^{22}\ \mathrm{cm}^{-3}. \quad (5)$$

The rate (4) was extracted from time spectra of delayed X-rays emitted in the 1S transfer reaction (3). These spectra were found to have a long-lived single exponential component following a prompt peak caused by muons directly captured in neon. Such a structure means that at the above-indicated pressures most of $\mu p(1S)$ atoms come into the transfer reaction after a quick thermalization in the gas mixture. So, the result (4) corresponds to thermalized muonic atoms. Then a typical 1S transfer cross-section at thermal energies is:

$$\sigma_t(1S) \sim 10^{-18}\ \mathrm{cm}^2. \quad (6)$$

The cross-section of the 2S transfer reaction (2) was estimated in [15,16]. At thermal energies it is:

$$\sigma_t(2S) \sim 3 \times 10^{-16}\ \mathrm{cm}^2. \quad (7)$$

So, the 2S transfer rate exceeds the rate of the 1S transfer background (3) by a factor of 300. This factor compensates the small ($\sim 1\%$) yield of the metastable $\mu p(2S)$ atoms.

Actually, in the PSI experiment [3,12] the contribution of the 1S transfer was additionally suppressed. $\mu p(2S)$ and $\mu p(1S)$ atoms were formed near the axis of a cylindrical chamber with the variable diameter around 1 cm and gold coated walls. The chamber was filled with a hydrogen-neon mixture at pressures of 4−16 mbar and neon concentrations of 3−50%. The cross-section of the $\mu p(1S)$ scattering by hydrogen molecules is around $10^{-18}\ \mathrm{cm}^2$ [17] while for $\mu p(2S)$ scattering it is about two orders of magnitude greater [6,7]. As a result, the free path of $\mu p(1S)$ atoms appreciably exceeds the chamber radius while for $\mu p(2S)$ atoms the relation is opposite. Accordingly, most of $\mu p(1S)$ atoms rapidly reach the chamber walls without scattering by hydrogen molecules[4]. On the contrary, the $\mu p(2S)$ atoms are quickly thermalized and disappear inside the chamber. For these reasons the measured time spectra of μNe X-rays consisted of the prompt peak followed by a rapidly dying component caused mostly by the 1S transfer, and a long-lived tail extending to several μs and contributed by the 2S transfer. Additional data on $\mu p(1S)$ atoms were obtained by recording time spectra of μAu X-rays emitted after these atoms had reached the chamber walls and transferred the muon to gold. The neon and gold time spectra were reproduced by a Monte Carlo simulation using the initial μp energy distribution measured in [10]. It was found to be impossible to fit the spectra with the help of the energy-independent 1S transfer rate (4) reduced to experimental neon densities (about $5 \times 10^3\ \mathrm{s}^{-1}$ at the partial neon pressure of 1 mbar). A five times greater value of this rate is needed, or its energy dependence has to be introduced. Concerning the 2S transfer, its taking into account is certainly needed to reproduce the long-lived tail of the neon time spectra. This directly indicates the existence of metastable $\mu p(2S)$ atoms. Their amount was found to be about the expected value of 1% per one muon stop. However, the slope of the long-lived tail proved to be independent on the partial neon pressure. This means that the 2S transfer rate actually observed is much less than the value expected on the basis of the theoretical estimation (7). The latter is of the order of $10^6\ \mathrm{s}^{-1}$ at 1 mbar of neon.

[4] If the collisions are ignored, the time spent by the muonic atom with the energy of 1 eV to pass 1 cm is about 0.8 μs.

1.3 The subject of the present work

In this paper we shall concentrate on the reaction (3) of the muon transfer from the 1S state of muonic protium to neon. As it was mentioned above, the PSI experiment on searching for the 2S state metastability was based on the fact of the strong suppression of this reaction at thermal energies. However, in the experiment most of $\mu p(1S)$ atoms were not thermalized, but passed through the target chamber without scattering on H_2 molecules so that their energy distribution remained close to the initial one. The latter was established to be rather extended [10]. For example, at 4 mbar of H_2 about 30% of the $\mu p(1S)$ atoms initially formed has the kinetic energy below 1 eV, and about 90% has the energy below 15 eV. So, the knowledge of the energy dependence of the 1S transfer cross-section seems to be significant. Here we try to make a contribution to surmounting this problem. Actually, the total cross-section $\sigma_t(1S)$ of the reaction (3) is calculated in the interval $10^{-4}\ \mathrm{eV} \le E_c \le 15\ \mathrm{eV}$. E_c is the collision energy (the initial kinetic energy in the center-of-mass frame). The lowest value of 10^{-4} eV corresponds to the temperature of a hydrogen-neon mixture around 1 K. Such low energies are considered in connection with measurements performed in liquid mixtures (see below). Besides the muon transfer, the elastic scattering of $\mu p(1S)$ atoms by neon is treated. It may be of interest because some of the hydrogen-neon mixtures studied in the PSI experiment had a high percentage of neon (up to 50%).

1.3.1 Some data on the muon transfer

Before coming to our calculations it is useful to discuss available data on the reaction (3). It is a particular case of the direct muon transfer from hydrogen to a chemical element with the atomic number Z:

$$\mu\mathrm{H}\,(1S) + Z \to \mu Z + \mathrm{H}. \quad (8)$$

H denotes a hydrogen isotope. Some features of this reaction for elements with $Z \geq 6$ were theoretically established in [15,18]. The muon transfer was treated to occur due to crossings and quasicrossings of adiabatic terms originating from the 1S state of muonic hydrogen and excited states of the μZ atom. The probability of nonadiabatic transitions from one term to another was estimated with the Landau-Zener formula. The interference of waves describing the relative motion in different channels was fully ignored. The collision energy was assumed to be small so that only the S-wave was taken into account. Before discussing the predictions made within these approximations let us introduce two quantities relevant to the reaction (8).

$$q_t(1\mathrm{S}) = N_{\mathrm{H}}\, v\, \sigma_t(1\mathrm{S}) \tag{9}$$

is the transfer rate for a fixed value of the velocity v of the relative motion of the μH and Z atoms. It is reduced to the atomic density of liquid hydrogen (5).

$$\lambda_t(1\mathrm{S}) = \langle q_t(1\mathrm{S}) \rangle \tag{10}$$

is the reduced rate of the muon transfer from thermalized μH atoms. The brackets mean averaging over the thermal motion. In a gas averaging is made over the Maxwellian distribution. In particular, the result (4) relates to this case.

The predictions mentioned above are [19]:

1. at collision energies corresponding to room temperatures the transfer cross-section is proportional to the following combination:

$$\sigma_t(1\mathrm{S}) \propto \frac{Z}{v\sqrt{M_n}}. \tag{11}$$

   M_n is the reduced mass of the nuclei H and Z. As the inverse v law is valid for the cross-section, the rate $q_t(1\mathrm{S})$ is energy independent, and $\lambda_t(1\mathrm{S})$ is temperature independent. The Z-dependence of the rates is monotone (linear in Z like in (11) or $\propto Z^{2/3}$ with taking into account the electron screening). The dependence on M_n indicates that the ratio of the transfer rates from thermalized μp and μd atoms is about 1.4;
2. at higher collision energies the transfer cross-section becomes inversely proportional to M_n and E_c:

$$\sigma_t(1\mathrm{S}) \propto \frac{1}{M_n E_c}. \tag{12}$$

   In this case the ratio of the μp and μd transfer rates at the same collision energy is about 2;
3. states of the μZ atom, the wave functions of which are stretched along the H$-Z$ axis, are mostly populated in the reaction (8). As a result, high-order components of the delayed K-series X-rays caused by the muon transfer are appreciably more intensive than those emitted by the μZ atoms formed directly.

The reaction (8) was experimentally studied in a number of dense gaseous targets at room temperatures [20]. The predictions on the monotone Z-dependence and on the relation of the transfer rates from μp and μd atoms were established to be valid only for heavy elements like Ar, Kr and Xe. In the region $6 \leq Z \leq 10$ the situation proved to be much more complicated. It was found that the Z-dependence was substantially nonmonotonic and the transfer from μd atoms occurred with an appreciably greater rate than from μp atoms. The discrepancy between the experimental results and the theoretical predictions is extreme for the muon transfer to neon. In this case the transfer rate from thermalized μp atoms evaluated in [15] exceeds the experimental value (4) by a factor of 10−15. The transfer rate from thermalized μd atoms was also measured. It is [14]:

$$\lambda_t^{\mu d}(1\mathrm{S}) = (1.010 \pm 0.026) \times 10^{11}\ \mathrm{s}^{-1}. \tag{13}$$

Contrary to the expectations, it is one order of magnitude greater than (4). Concerning the inverse v law (11) for the transfer cross-section, it appears to be invalid at room temperatures. This follows from the comparison of the rates (4) and (13) measured in gaseous targets at 300 K and the transfer rates observed in liquid hydrogen-neon mixtures near 20 K. The latter are [20]:

$$\lambda_t^{\mu p}(1\mathrm{S}) = (0.300 \pm 0.100) \times 10^{11}\ \mathrm{s}^{-1}, \tag{14}$$

$$\lambda_t^{\mu d}(1\mathrm{S}) = (1.8 \pm 0.7) \times 10^{11}\ \mathrm{s}^{-1}. \tag{15}$$

The temperature dependence of the transfer rates is clearly seen. This may mean that the quantity $q_t(1\mathrm{S})$ is not constant at the collision energies below, for example, (1/40) eV. However, a reserve should be done here. At temperatures about 20 K typical de Broglie wavelengths of μp and μd atoms are comparable with distances between H_2 molecules in liquid hydrogen. For this reason the wave describing the relative motion of muonic and neon atoms may be distorted due to scattering on surrounding H_2 molecules. This effect may additionally change the transfer rate.

A possible explanation of the nonmonotonic Z-dependence as well as the unexpected ratio of the μp and μd transfer rates was suggested in [21]. The interference of waves describing the relative motion in different channels was revealed to be very significant. The fact is that the WKB approximation, on which the standard Landau-Zener formula is based, may be not applicable in the case of the muon transfer to light elements. Indeed, the well-known parameter $(d\lambda/dr)$ evaluated in relevant crossing points is not very small. A modification of the Landau-Zener formula for such a case was made in [21]. The other approximations coincided practically with those used in [15,18]. It was found in this way that the transfer rate was an oscillating function of the dimensionless parameter

$$\zeta = [2(d\lambda/dr)]^{-2/3}. \tag{16}$$

The right side of this formula is taken in the crossing point which makes the main contribution to the muon transfer. At thermal energies the parameter ζ is:

$$\zeta = \left(\frac{3Z\sqrt{2M_n}}{8r_c}\right)^{2/3}. \tag{17}$$

Here the mass M_n and the internuclear distance r_c corresponding to the crossing point are expressed in muon-atom units (m.a.u. in short):

$$\hbar = e = m_\mu = 1, \tag{18}$$

e is the proton charge, m_μ is the muon mass, the length and energy units are respectively equal to 2.56×10^{-11} cm and 5.63 keV. The relation (17) means that the transfer rate oscillates with changing Z and M_n. For heavy element $\zeta \gg 1$, and the WKB approximation is applicable. For light elements the values of ζ are around unity, and the oscillations are significant. For example, ζ found for the transfer from μp to neon is very close to the position of a minimum of the transfer rate. Accordingly, this reaction is suppressed. The transfer from μd to neon is much faster because the corresponding ζ is close to the position of a maximum. The numerical values of the transfer rate to neon obtained in [21] are in a reasonable agreement with the experimental values (4) and (13). Good results were also obtained for the transfer to N and O [19]. Concerning the dependence of the transfer cross-section on the relative velocity predicted in [21], the inverse v law was again derived for thermal energies. So, the difference of the transfer rates to neon measured in the gaseous and liquid mixtures remained unexplained. In the subsequent paper [22] the transfer to light elements was treated at $E_c \sim 0.2$ eV by adding the contribution of the P-wave. However, the S-wave transfer cross-section was found to be still proportional to v^{-1}. This result contradicts the expected dependence (12).

Recently the muon transfer from hydrogen isotopes to some elements was treated on the basis of integro-differential Faddeev-Hahn-type equations [23,24]. The calculations were made within the two-state approximation, i.e. only the 1S state of muonic hydrogen and one state of the μZ atom were taken into account in the reaction (8). The muon charge distribution in the entrance and transfer channels was described with hydrogenlike bound-state wavefunctions. Only the S-wave in the entrance channel was considered. The electron screening was not introduced. The transfer rate evaluated within this approach proved to be in a good agreement with experimental results. In particular, the rate (13) of the muon transfer from deuterium to neon was reasonably reproduced. The transfer from protium to neon was not treated. One should make a few remarks on these papers. An important advantage of the method used there is the correct description of the relative motion of the fragments at large interatomic separations in both the entrance and transfer channels. This is achieved due to each channel being described in the proper Jacobi coordinates. However, some disadvantages should be indicated. The first one is the use of the hydrogenlike muon wavefunctions. In this case the muon charge distribution in each channel is frozen, it is not changed as the fragments approach each other. Such a situation seems to be unsatisfactory in describing the entrance channel because the polarization of the charge cloud of muonic hydrogen in the Coulomb field of the Z-atom is fully ignored. In particular, the polarization leads to the appearance of the well-known long-range attraction. If the electron screening is not taken into account, the corresponding potential is (in muon-atom units):

$$U_p(R) = -\frac{\beta Z^2}{2R^4}. \tag{19}$$

β is the dipolar polarizability of μH, R is the distance between the nucleus Z and the center of mass of μH. It may be expected that this attraction is very significant at low collision energies. For example, according to [21], the quasicrossing of terms responsible for the muon transfer from protium to neon occurs at $R \sim 26$ m.a.u. The formula (19) yields U_p about 4 eV. This is much greater than thermal energies. Moreover, because of its long-range nature this attraction appreciably changes the S-wave phase. The authors of [23,24] could not obtain the potential (19) in any natural way and had to add it artificially. In principle, the polarization may be partly taken into account within their method. At least the 2P state of muonic hydrogen should be included into consideration. However, this way does not look attractive. Indeed, the polarization is significant at low collision energies, but its description needs the addition of the 2P state with the excitation energy of 2 keV. It should be also noted that the authors of the papers discussed used an incorrect value of the dipolar polarizability. They took $\beta = 9/2$ m.a.u. while the correct value is:

$$\beta = \frac{9}{2m_{\mu\mathrm{H}}^3}. \tag{20}$$

$m_{\mu\mathrm{H}}$ is the reduced mass of muonic hydrogen. The presence of its cube in the denominator of this formula follows from the definition of β:

$$\beta = 2\sum_k \frac{|(d_z)_{0k}|^2}{E_k - E_0}. \tag{21}$$

d_z is the projection of the dipole moment of the μH atom on the direction of an external field, k labels the atomic P-states, the subscript 0 means the 1S state, E_0 and E_k are the energies of the corresponding states. As the atomic wavefunctions involve the reduced mass of μH, the square of the dipole matrix element is proportional to $m_{\mu\mathrm{H}}^{-2}$. One more power of this mass appears in the energy denominator. The factor $m_{\mu\mathrm{H}}^{-3}$ in (20) is especially significant for muonic protium. In this case

$$\beta \approx 6.20, \tag{22}$$

instead of 4.5 used in [23,24]. One more disadvantage of these papers is the neglect of the electron screening. According to [15], the electron screening in the entrance channel of the reaction (8) reduces the transfer cross-section by a factor of $Z^{1/3}$. For the transfer to neon it is about 2.

1.3.2 A preliminary discussion of the present method

The consideration presented above shows that an adequate description of the entrance channel of the transfer

reaction should include effects of the muon charge cloud polarization. This may be achieved by using two-center muon wavefunctions. A realization of such an approach called the perturbed stationary state (PSS) method is well-known [25]. The three-body problem is formulated in coordinates describing the muon motion in the field of two fixed nuclei. For the reaction (8) these are the vector $\mathbf{R}_{\mathrm{H}Z}$ joining the nuclei H and Z and the vector connecting the midpoint of $\mathbf{R}_{\mathrm{H}Z}$ with the muon. The use of these coordinates seems to be inconvenient because they describe the relative motion of the fragments at large separations in neither of the binary channels. A more attractive way was suggested in treating the muon transfer between hydrogen isotopes [26]. Each binary channel was considered in its natural Jacobi coordinates corresponding to the asymptotic separation into the fragments. The problem of the muon motion in the field of two fixed Coulomb centers (the two-center problem) was separately formulated in each of the channels. The three-body wavefunction was expanded in solutions of these problems. Finally, a set of coupled integro-differential equations for relative motion functions was obtained. So, this approach provides the asymptotically correct description of the binary channels. As the two-center muon wavefunctions are used, the muon charge distribution in each of the channels is flexible. It is adiabatically deformed as the distance between the fragments changes so that polarization effects are taken into consideration. Moreover, the migration of the muon charge from one nucleus to another caused by quasicrossings of adiabatic two-center terms is also included. This feature seems to be very important for the muon transfer. Unfortunately, a practical realization of this method needs solving a complicated set of coupled integro-differential equations. For this reason we use a simplified approach. As low collision energies are also of interest for us, the entrance channel is described as accurately as possible. Similarly to [26], the Jacobi coordinates relating to this channel are used, and the two-center problem is formulated in these coordinates. This way will be seen to provide the correct dissociation limit in the entrance channel and the polarization attraction (19) with the correct dipolar polarizability (22). No spurious long-range interactions appear in this channel. Moreover, the electron screening is easily introduced. Our main simplification is the use of a group of solutions of the above two-center problem for describing the transfer channel. These solutions are localized at the heavier Coulomb center in the separated atoms limit, and, in this sense, somehow describe the muon transfer. However, their use means that the transfer channel is treated in the Jacobi coordinates of the entrance channel. Actually, the two-center solutions discussed are not correlated to any individual states of the μZ atom. Of course, a number of the well-known difficulties arise immediately. The dissociation limits in the transfer channel are incorrect, and spurious long-range potentials appear there. It is clear that the partial transfer cross-sections to individual states of the μZ atom can not be obtained in this way. However, on the whole a group of solutions localized asymptotically at the heavier Coulomb center may be considered to describe the transition from the entrance channel to the transfer one, and the total transfer cross-section may be evaluated. Actually, this is reduced to solving a set of coupled ordinary differential equations for relative motion functions. Unlike the standard PSS method [25] in which the correct asymptotic description of both the entrance and transfer channels meets serious difficulties (incorrect dissociation limits, etc.), the present approach drives these difficulties into the transfer channel. This seems to be reasonable because the relative motion energies in the transfer channel are much greater than the collision energy in the entrance one. For example, the analysis of energy spectra of the delayed K-series X-rays made in [14] for the muon transfer from protium to neon indicates that states of muonic neon with the principle quantum number $n = 6$ are initially populated. In this case the relative motion energy in the transfer channel is about 5.2 keV.

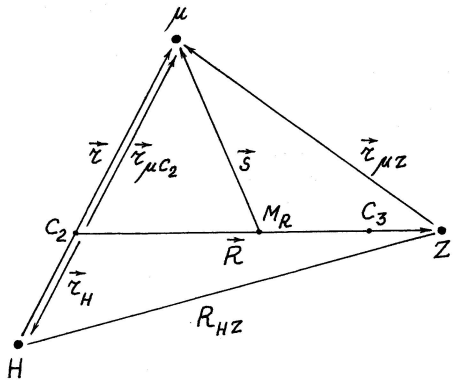

Fig. 1. The Jacobi coordinates of the entrance channel and relevant notations. C_3 is the center of mass of the three-body system, C_2 is the one of the pair μH, M_R is the midpoint of the vector $\mathbf{R}$.

2 The formalism

2.1 The choice of variables in the Coulomb three-body problem

Muon-atom units (18) are used in this section. First, let us consider the system consisting of a negative muon μ and two pointlike nuclei H and Z (Fig. 1). In the center-of-mass frame of this system its Hamiltonian is[5]:

$$\hat{H} = -\frac{1}{2M_r}\,\Delta_{\mathbf{R}} + \hat{H}_\mu + \frac{Z}{R_{\mathrm{H}Z}}, \tag{23}$$

$$\hat{H}_\mu = -\frac{1}{2m_{\mu\mathrm{H}}}\,\Delta_{\mathbf{r}} - \frac{1}{r} - \frac{Z}{r_{\mu Z}}. \tag{24}$$

The vectors $\mathbf{R}$ and $\mathbf{r}$ are the Jacobi coordinates of the entrance channel of the reaction (8). $\mathbf{r}$ joins the nucleus H and the muon, $\mathbf{R}$ connects the center of mass of the pair μH with the nucleus Z. M_r is the reduced mass of the nucleus Z with respect to μH:

$$M_r^{-1} = (M_{\mathrm{H}} + 1)^{-1} + M_Z^{-1}, \tag{25}$$

[5] The fine and hyperfine structure effects are ignored.

$M_{\rm H}$ and M_Z are the nuclear masses. $m_{\mu{\rm H}}$ is the reduced mass of muonic hydrogen:

$$m_{\mu{\rm H}}^{-1} = M_{\rm H}^{-1} + 1. \tag{26}$$

$R_{{\rm H}Z}$ and $r_{\mu Z}$ are the distances between the particles indicated in the subscripts.

The part H_μ of the Hamiltonian may be rewritten as follows [26]:

$$\hat{H}_\mu = m_{\mu{\rm H}}\,\hat{h}_\mu, \tag{27}$$

$$\hat{h}_\mu = -\frac{1}{2}\,\Delta_{\mathbf{s}} - \frac{1}{|\mathbf{s}+\frac{\mathbf{R}}{2}|} - \frac{Z'}{|\mathbf{s}-\frac{\mathbf{R}}{2}|}. \tag{28}$$

The vector $\mathbf{s}$ is directed from the midpoint of $\mathbf{R}$ to the muon (Fig. 1):

$$\mathbf{s} = m_{\mu{\rm H}}\,\mathbf{r} - \frac{\mathbf{R}}{2}. \tag{29}$$

The quantity Z' is:

$$Z' = \frac{Z}{m_{\mu{\rm H}}}. \tag{30}$$

$\hat{h}_\mu$ is seen to be the Hamiltonian of the muon in the field of two fixed Coulomb centers, the charges of which are equal to unity and Z'. The unit charge is placed in the center of mass of the pair μH, the position of the charge Z' coincides with the one of the nucleus Z. For the muon transfer from protium to neon

$$Z' \approx 11.1. \tag{31}$$

The three-body Hamiltonian $\hat{H}$ may be also written in the Jacobi coordinates of the transfer channel, and a two-center Hamiltonian similar to $\hat{h}_\mu$ may be separated there. In this case the charges of the Coulomb centers are equal to Z and $m_{\mu Z}^{-1}$ ($m_{\mu Z}$ is the reduced mass of the μZ atom). The former is placed in the center of mass of μZ, the position of the latter coincides with the one of the hydrogen nucleus. An expansion of the three-body wavefunction in a finite set of eigenstates of these two-center Hamiltonians seems to be a good approximation for the transfer reaction. However, as it was explained in Section 1.3.2, only eigenstates of $\hat{h}_\mu$ are used in our simplified approach.

The vectors $\mathbf{R}$ and $\mathbf{r}$ are initially related to a Cartesian coordinate frame K, the axes of which are somehow fixed and the origin is the center of mass of the three-body system. It should be noted that this center lies at the vector $\mathbf{R}$ (Fig. 1). Let (R, Θ, Φ) be the spherical coordinates of $\mathbf{R}$ in the frame K. In our problem it is convenient to use another frame K', the z-axis of which is directed along $\mathbf{R}$. It is obtained from K by the rotation through the Eulerian angles (Φ, Θ, 0). The origins of K and K' coincide. The Cartesian components of the vector $\mathbf{r}$ in the frames K' and K are related as follows:

$$\begin{cases} x' = x\cos\Theta\cos\Phi + y\cos\Theta\sin\Phi - z\sin\Theta\,, \\ y' = \quad -x\sin\Phi \quad + \quad y\cos\Phi\,, \\ z' = x\sin\Theta\cos\Phi + y\sin\Theta\sin\Phi + z\cos\Theta\,. \end{cases} \tag{32}$$

One more relevant frame K'' is obtained from K' by the translation of the origin to the midpoint of $\mathbf{R}$. The x- and y-axis of K'' are parallel to the ones of K', the z-axis is common. The eigenstates of $\hat{h}_\mu$ are constructed in prolate spheroidal coordinates of the muon defined in K'':

$$\xi = \frac{(r_{\mu C_2} + r_{\mu Z})}{R}; \quad \eta = \frac{(r_{\mu C_2} - r_{\mu Z})}{R}. \tag{33}$$

$r_{\mu C_2}$ and $r_{\mu Z}$ are the distances from the muon to the center of mass of μH and the nucleus Z respectively (Fig. 1). The third spheroidal coordinate is the azimuthal angle φ lying in the xy-plane of K''. The coordinates of the center of mass of the pair μH where the fixed unit charge involved into $\hat{h}_\mu$ is placed are: $\xi = +1$, $\eta = -1$. The coordinates of the charge Z' are: $\xi = +1$, $\eta = +1$. The Cartesian components of the vector $\mathbf{r}$ in the frame K' are expressed in terms of ξ, η and φ as follows:

$$\begin{cases} x' = r_\perp \cos\varphi, \\ y' = r_\perp \sin\varphi, \\ z' = R'(1+\xi\eta). \end{cases} \tag{34}$$

The quantities $r_\perp$ and R' are:

$$r_\perp = R'\sqrt{(\xi^2-1)(1-\eta^2)}; \quad R' = \frac{R}{2m_{\mu{\rm H}}}. \tag{35}$$

The eigenstates of $\hat{h}_\mu$ are functions of the spheroidal coordinates and satisfy the equation:

$$\hat{h}_\mu\,\psi_{jm}(\xi,\eta;R)\,\frac{\exp(\pm im\varphi)}{\sqrt{2\pi}} = \varepsilon_{jm}(R)\,\psi_{jm}(\xi,\eta;R)\,\frac{\exp(\pm im\varphi)}{\sqrt{2\pi}}. \tag{36}$$

The dependence on φ is explicitly indicated here. The non-negative integer m is the modulus of the magnetic quantum number, the subscript j denotes a set of the other quantum numbers needed to specify the state. For a bound state these are the numbers n_ξ and n_η of nodes in the variables ξ and η or the parabolic quantum numbers n_1 and n_2 in the limit $R \to \infty$ [25,27]. $\varepsilon_{jm}(R)$ is the eigenvalue of $\hat{h}_\mu$. The equation (36) is solved at a fixed R so that R is involved in the eigenstates as a parameter. The real functions $\psi_{jm}(\xi,\eta;R)$ with the same m are orthonormal:

$$\int \psi_{im}(\xi,\eta;R)\,\psi_{jm}(\xi,\eta;R)\,d\tau = \delta_{ij}; \quad d\tau = (R/2)^3\,(\xi^2-\eta^2)\,d\xi\,d\eta. \tag{37}$$

The integration region is: $1 \le \xi < \infty$; $-1 \le \eta \le +1$. The orthonormalization with respect to the magnetic quantum number is due to the factors $\exp(\pm im\varphi)/\sqrt{2\pi}$.

Let the wavefunction of the three-body system be initially specified as a function of the components of the vectors $\mathbf{R}$ and $\mathbf{r}$ in the coordinate frame K. The inversion of (32) and the relations (34) allow one to transform it to the new variables (R, Θ, Φ, ξ, η, φ). Accordingly,

the transition to these variables is to be done in the three-body Hamiltonian (23). First of all this concerns the operator $\Delta_{\mathbf{R}}$ which initially includes partial derivatives with respect to the components of $\mathbf{R}$ at fixed values of the ones of $\mathbf{r}$ in the frame K. In transforming this operator we follow the convenient formalism developed in [28]. It should be emphasized that our final results differ from those obtained in [28] because of another choice of the three-body coordinates. The transformation is made in two steps. At the first one the variables (R, Θ, Φ, x', y', z') are introduced with the help of (32). The operator $\Delta_{\mathbf{R}}$ is split into two terms specified by different selection rules with respect to the magnetic quantum number m:

$$\Delta_{\mathbf{R}} = \Delta_0 + \Delta_1. \tag{38}$$

The first term does not change m:

$$\Delta_0 = \frac{\partial'^2}{\partial R^2} + \frac{2}{R}\frac{\partial'}{\partial R} - \frac{1}{R^2}\left(\hat{\mathbf{J}}^2 + \hat{\mathbf{l}}^2 - 2\hat{l}_{z'}^2\right). \tag{39}$$

The prime denotes the differentiation at fixed (x', y', z'). $\hat{\mathbf{J}}^2$ is the square of the operator $\hat{\mathbf{J}}$ of the orbital angular momentum of the three-body system with respect to its center of mass:

$$\hat{\mathbf{J}} = \hat{\mathbf{L}} + \hat{\mathbf{l}}; \quad \hat{\mathbf{L}} = -i\,[\mathbf{R}\times\nabla_{\mathbf{R}}]; \quad \hat{\mathbf{l}} = -i\,[\mathbf{r}\times\nabla_{\mathbf{r}}]. \tag{40}$$

$\hat{\mathbf{l}}^2$ is the square of the vector $\hat{\mathbf{l}}$, $\hat{l}_{z'}$ is its z-component in the frame K'. In terms of the variables considered the components of $\hat{\mathbf{J}}$ in the frame K' are:

$$\hat{J}_{x'} = \frac{i}{\sin\Theta}\frac{\partial'}{\partial\Phi} + \cot\Theta\,\hat{l}_{z'}; \quad \hat{J}_{y'} = -i\frac{\partial'}{\partial\Theta}; \quad \hat{J}_{z'} = \hat{l}_{z'}. \tag{41}$$

In the frame K we have:

$$\hat{J}_{\pm} = \exp(\pm i\,\Phi)\left(\pm\frac{\partial'}{\partial\Theta} + i\,\cot\Theta\frac{\partial'}{\partial\Phi} + \frac{\hat{l}_{z'}}{\sin\Theta}\right);$$
$$\hat{J}_z = -i\frac{\partial'}{\partial\Phi}. \tag{42}$$

Here $\hat{J}_{\pm} = \hat{J}_x \pm i\hat{J}_y$. The Cartesian components of $\hat{\mathbf{J}}$ in the frames K' and K are related similarly to (32). The operator $\hat{\mathbf{J}}^2$ is:

$$\hat{\mathbf{J}}^2 = -\left[\frac{1}{\sin\Theta}\frac{\partial'}{\partial\Theta}\sin\Theta\frac{\partial'}{\partial\Theta} + \left(\frac{1}{\sin\Theta}\frac{\partial'}{\partial\Phi} - i\,\hat{l}_{z'}\cot\Theta\right)^2\right] + \hat{l}_{z'}^2. \tag{43}$$

The second term in (38) varies m by unity:

$$\Delta_1 = \frac{2}{R^2}\left(\hat{\mathbf{l}}\hat{\mathbf{J}} - \hat{l}_{z'}^2\right) = \frac{2}{R^2}\left(\hat{l}_{x'}\hat{l}_{z'}\cot\Theta - i\,\hat{l}_{y'}\frac{\partial'}{\partial\Theta} + \frac{i\,\hat{l}_{x'}}{\sin\Theta}\frac{\partial'}{\partial\Phi}\right). \tag{44}$$

$\hat{l}_{x'}$ and $\hat{l}_{y'}$ are the x- and y-components of $\hat{\mathbf{l}}$ in the frame K'. The term $(-\Delta_1/2M_r)$ in the three-body Hamiltonian describes the Coriolis interaction.

The second step is the transition to the variables (R, Θ, Φ, ξ, η, φ) with the help of (34). The operators introduced above are transformed as follows:

$$\frac{\partial'}{\partial R} = \frac{\partial}{\partial R} + \frac{\hat{d}}{R}. \tag{45}$$

The R-differentiation in the right side of this formula is made at fixed values of the spheroidal coordinates. The operator $\hat{d}$ is:

$$\hat{d} = -\frac{1}{(\xi-\eta)}\left[\left(\xi^2-1\right)\frac{\partial}{\partial\xi} + \left(1-\eta^2\right)\frac{\partial}{\partial\eta}\right]. \tag{46}$$

The partial derivatives with respect to the spheroidal coordinates are evaluated at fixed (R, Θ, Φ) so that $\partial/\partial R$ and $\hat{d}$ are commutative. The second R-derivative involved into (39) is obtained by applying (45) twice. The components of $\hat{\mathbf{l}}$ take the form:

$$\hat{l}_{\pm} = \exp(\pm i\varphi)\left(\pm\hat{a} + i\,\hat{b}\,\frac{\partial}{\partial\varphi}\right); \quad \hat{l}_{z'} = -i\,\frac{\partial}{\partial\varphi}. \tag{47}$$

Here $\hat{l}_{\pm} = \hat{l}_{x'} \pm i\hat{l}_{y'}$, and the operators $\hat{a}$ and $\hat{b}$ are:

$$\hat{a} = \frac{\sqrt{(\xi^2-1)(1-\eta^2)}}{(\xi-\eta)}\left(\frac{\partial}{\partial\xi} - \frac{\partial}{\partial\eta}\right);$$
$$\hat{b} = \frac{1+\xi\eta}{\sqrt{(\xi^2-1)(1-\eta^2)}}. \tag{48}$$

The square of $\hat{\mathbf{l}}$ is:

$$\hat{\mathbf{l}}^2 = \left(\hat{b}^2+1\right)\hat{l}_{z'}^2 - \left(\hat{a}+\hat{b}\right)\hat{a}. \tag{49}$$

Concerning the derivatives with respect to the angles Θ and Φ involved into (41–44), they are now evaluated at fixed spheroidal coordinates. Indeed, the relations (34) do not involve these angles so that no additional transformation of the derivatives is needed. The two-center Hamiltonian $\hat{h}_\mu$ is expressed in terms of the spheroidal coordinates in the standard way [25]. Finally, the distance $R_{\mathrm{H}Z}$ involved into the Coulomb repulsion of the nuclei is:

$$R_{\mathrm{H}Z} = R\sqrt{\left(\frac{\xi+\eta}{2M_{\mathrm{H}}}\right)^2 + \frac{(1+\xi\eta)}{M_{\mathrm{H}}} + 1}. \tag{50}$$

The above-mentioned differences of the present results from those obtained in [28] are particularly manifested in the structure of the operators $\hat{d}$, $\hat{a}$ and $\hat{b}$. Moreover, as the authors of [28] did not use any Jacobi coordinates, they had a number of additional terms in the three-body Hamiltonian. For example, the operator $(\nabla_{\mathbf{R}}\nabla_{\mathbf{r}} + \nabla_{\mathbf{r}}\nabla_{\mathbf{R}})$ appeared. Such terms are absent in the present consideration.

2.2 Basis functions

The three-body Hamiltonian commutes with the operators $\hat{\mathbf{J}}^2$, $\hat{J}_z$ as well as with the operator $\hat{\mathrm{P}}$ of the coordinate inversion. A convenient basis in which the three-body wavefunction may be expanded consists of eigenstates of these three operators. We additionally demand the basis functions to be eigenstates of the two-center Hamiltonian $\hat{h}_\mu$. Before constructing this basis let us consider how the variables $(R, \Theta, \Phi, \xi, \eta, \varphi)$ are transformed under the inversion. The inversion reverses the sign of the Cartesian components of the vectors $\mathbf{R}$ and $\mathbf{r}$ in the frame K. The transformation of the angles Θ and Φ is obvious:

$$\begin{cases} \Theta \to \pi - \Theta, \\ \Phi \to \pi + \Phi. \end{cases} \tag{51}$$

The relations (32) yield:

$$\begin{cases} x' \to -x', \\ y' \to y', \\ z' \to z'. \end{cases} \tag{52}$$

The transformation of the spheroidal coordinates follows from (34):

$$\begin{cases} \xi \to \xi, \\ \eta \to \eta, \\ \varphi \to \pi - \varphi. \end{cases} \tag{53}$$

As only the angular variables are changed, the problem is to construct angular functions which are eigenstates of $\hat{\mathbf{J}}^2$, $\hat{J}_z$ and $\hat{\mathrm{P}}$. Let us consider the Wigner function $D^J_{Mm}(\Phi, \Theta, \varphi)$ which is the eigenstate of $\hat{\mathbf{J}}^2$, $\hat{J}_z$ and $\hat{J}_{z'} = \hat{l}_{z'}$ with the eigenvalues $J(J+1)$, M and m [29]. It is transformed under the inversion as follows:

$$D^J_{Mm}(\Phi, \Theta, \varphi) \to (-1)^{J-m} D^J_{M(-m)}(\Phi, \Theta, \varphi). \tag{54}$$

If $m \neq 0$, the Wigner functions involved here are different, and the angular functions required are their even and odd combinations. It is convenient to specify these combinations as follows:

$$\Upsilon^{JP}_{Mm}(\Phi, \Theta, \varphi) = \frac{\sqrt{2J+1}}{4\pi} \Big[(-1)^m D^J_{Mm}(\Phi, \Theta, \varphi) + P(-1)^J D^J_{M(-m)}(\Phi, \Theta, \varphi) \Big]. \tag{55}$$

$P = \pm(-1)^J$ is the eigenvalue of the operator $\hat{\mathrm{P}}$:

$$\hat{\mathrm{P}}\, \Upsilon^{JP}_{Mm} = P\, \Upsilon^{JP}_{Mm}. \tag{56}$$

Υ^{JP}_{Mm} is also the eigenstate of $\hat{l}^2_{z'}$ (but not $\hat{l}_{z'}$) with the eigenvalue m^2. The functions (55) are orthonormal:

$$\int_0^\pi \sin\Theta\, d\Theta \int_0^{2\pi} d\Phi \int_0^{2\pi} d\varphi \left(\Upsilon^{JP}_{Mm}\right)^* \Upsilon^{J'P'}_{M'm'} = \delta_{JJ'}\, \delta_{PP'}\, \delta_{MM'}\, \delta_{mm'}. \tag{57}$$

If $m = 0$, both the Wigner functions in (54) are reduced to the ordinary spherical function $Y_{JM}(\Theta, \Phi)$ so that the dependence on φ disappears and the angular functions satisfying the conditions (56, 57) are:

$$\Upsilon^{JP}_{Mm=0}(\Phi, \Theta, \varphi) = \frac{Y_{JM}(\Theta, \Phi)}{\sqrt{2\pi}}. \tag{58}$$

In this case the parity is unambiguously specified by the quantum number J: $P = (-1)^J$.

So, our basis functions have the structure:

$$\Psi^{JP}_{Mjm}(R, \Theta, \Phi, \xi, \eta, \varphi) = \frac{\chi^{JP}_{jm}(R)}{R}\, \Upsilon^{JP}_{Mm}(\Phi, \Theta, \varphi)\, \psi_{jm}(\xi, \eta; R). \tag{59}$$

$\chi^{JP}_{jm}(R)$ is a radial function depending on the indicated quantum numbers.

2.3 Coupled equations

In the center-of-mass frame of the three-body system the transfer reaction (8) is described by the Schrödinger equation:

$$\hat{H}\, \Psi = E\, \Psi. \tag{60}$$

The Hamiltonian $\hat{H}$ was introduced in (23). The energy E is:

$$E = E_{\mu\mathrm{H}}(1\mathrm{S}) + E_c. \tag{61}$$

The first term is the energy of the ground state of muonic hydrogen:

$$E_{\mu\mathrm{H}}(1\mathrm{S}) = -\frac{m_{\mu\mathrm{H}}}{2}. \tag{62}$$

The collision energy E_c is:

$$E_c = \frac{M_r v^2}{2}. \tag{63}$$

v is the velocity of the relative motion of the μH atom and the nucleus Z at infinite separation. The reduced masses $m_{\mu\mathrm{H}}$ and M_r were introduced in (25, 26).

The solution of the Schrödinger equation specified additionally by the quantum numbers J, M and P is sought in the form of an expansion in the basis functions (59):

$$\Psi^{JP}_M = \sum_{jm} \frac{\chi^{JP}_{jm}(R)}{R}\, \Upsilon^{JP}_{Mm}(\Phi, \Theta, \varphi)\, \psi_{jm}(\xi, \eta; R). \tag{64}$$

The sum is taken over all the quantum numbers (jm) of the two-center problem (36). The expansion is now substituted into the equation (60), the result is multiplied by a function $\left(\Upsilon^{JP}_{Mm'}\right)^* \psi_{im'}$ and integrated over the variables $(\Theta, \Phi, \xi, \eta, \varphi)$. This procedure yields the set of coupled

equations for the radial functions:

$$-\frac{1}{2M_r}\frac{d^2\chi^{JP}_{jm}}{dR^2}+\left\{\frac{\left[J(J+1)-2m^2\right]}{2M_rR^2}+U_{jm}(R)\right\}\chi^{JP}_{jm}+\sum_{i\neq j}\left\{W_{jm,im}(R)\,\frac{d\chi^{JP}_{im}}{dR}+\left[U^{(a)}_{jm,im}(R)+U^{(s)}_{jm,im}(R)\right]\chi^{JP}_{im}\right\}+\sum_i\sum_{m'=m\pm1}V_{jm,im'}(R)\,\chi^{JP}_{im'}=E_c\,\chi^{JP}_{jm}. \quad (65)$$

The matrix elements appeared here are combinations of integrals of two-center wavefunctions $\psi_{jm}(\xi,\eta;R)$ and their derivatives. The integrals are taken over the spheroidal coordinates ξ and η. The corresponding volume element $d\tau$ and the integration limits are specified in (2.1). We have:

$$W_{jm,im}(R)=-\frac{1}{2M_r}\int d\tau\left(\psi_{jm}\,\frac{\partial'\psi_{im}}{\partial R}-\psi_{im}\,\frac{\partial'\psi_{jm}}{\partial R}\right),$$
$$U^{(a)}_{jm,im}(R)=\frac{1}{2}\,\frac{dW_{jm,im}(R)}{dR}. \quad (66)$$

$\partial'/\partial R$ operates on the function $\psi_{im}(\xi,\eta;R)$ in accordance with (45). Both the two-center wavefunctions involved here have the same m. The matrices considered are antisymmetric:

$$W_{jm,im}(R)=-W_{im,jm}(R),$$
$$U^{(a)}_{jm,im}(R)=-U^{(a)}_{im,jm}(R). \quad (67)$$

The diagonal elements ($j=i$) vanish.

The next matrix element $U^{(s)}_{jm,im}(R)$ also couples the two-center wavefunctions with the same m. It is:

$$U^{(s)}_{jm,im}(R)=U^{(1)}_{jm,im}(R)+U^{(2)}_{jm,im}(R)+U^{(3)}_{jm,im}(R). \quad (68)$$

The first term is contributed by operators involved into (39):

$$U^{(1)}_{jm,im}(R)=\frac{1}{2M_r}\left[F_{jm,im}(R)+\frac{G_{jm,im}(R)}{R^2}\right],$$
$$F_{jm,im}(R)=\int d\tau\left(\frac{\partial'\psi_{jm}}{\partial R}\right)\left(\frac{\partial'\psi_{im}}{\partial R}\right),$$
$$G_{jm,im}(R)=\int d\tau\,(\hat a\psi_{jm})\,(\hat a\psi_{im})+m^2\left(\int d\tau\,\psi_{jm}\hat b^2\psi_{im}+\delta_{ji}\right). \quad (69)$$

The second term is the eigenstate of the Hamiltonian H_μ (27) counted from the energy of μH(1S):

$$U^{(2)}_{jm,im}(R)=\left[m_{\mu\mathrm{H}}\,\varepsilon_{jm}(R)-E_{\mu\mathrm{H}}(1\mathrm{S})\right]\delta_{ji}. \quad (70)$$

Finally, the third term is the matrix element of the Coulomb repulsion of the nuclei:

$$U^{(3)}_{jm,im}(R)=Z\int d\tau\,\frac{\psi_{jm}\,\psi_{im}}{R_{\mathrm{H}Z}}. \quad (71)$$

The matrix (68) is symmetric:

$$U^{(s)}_{jm,im}(R)=U^{(s)}_{im,jm}(R). \quad (72)$$

Its diagonal elements are separated in the set (65):

$$U_{jm}(R)\equiv U^{(s)}_{jm,jm}(R). \quad (73)$$

It is convenient to write them similarly to (68):

$$U_{jm}(R)=U^{(1)}_{jm}(R)+U^{(2)}_{jm}(R)+U^{(3)}_{jm}(R). \quad (74)$$

The diagonal elements of (69–71) are taken here.

The last sum in the left side of (65) involves the matrix elements of the Coriolis interaction which couples the functions ψ_{jm} and $\psi_{i(m\pm1)}$:

$$V_{jm,im'}(R)=-\frac{N_{m'}}{4M_rR^2}\,\delta_{m'(m\pm1)}\sqrt{(J\mp m)(J\pm m+1)}\times\left[\pm\int d\tau\left(\psi_{jm}\,\hat a\,\psi_{im'}-\psi_{im'}\,\hat a\,\psi_{jm}\right)+(2m\pm1)\int d\tau\,\psi_{jm}\,\hat b\,\psi_{im'}\right]. \quad (75)$$

The factor $N_{m'}=\sqrt{2}$ at $m'=0$, otherwise it is equal to unity.

The set of coupled equations (65) explicitly includes the quantum numbers J and m. The latter is involved into the two-center wavefunctions ψ_{jm} and, as a result, into the matrix elements. The parity quantum number P is formally absent in the equations. However, the structure of the set depends substantially on P. For example, at $J=0$ the two-center eigenstates with $m=0$ are involved only into the the expansion (64) of the even three-body wavefunction ($P=+1$). The expansion of the odd wavefunction ($P=-1$) does not include these states. Accordingly, the set of coupled equations is different in these cases.

2.4 The behaviour of matrix elements at large interatomic separations

2.4.1 The entrance channel

The main idea of the present approach is to provide the asymptotically correct description of the entrance channel of the transfer reaction (8) at large distances R. In this limit the bound eigenstates of the two-center problem (36) are divided into two groups. The states of one group are localized near the left center which has the unit charge and placed in the center-of-mass of the μH atom (Fig. 1). The other states are localized near the right center Z' (30). The simplest way to describe the entrance channel is to take into account the only state of the left-center group in the expansion (64). The quantum numbers of this state are:

$$m=n_1=n_2=0;\quad n=1. \quad (76)$$

n_1 and n_2 are the parabolic quantum numbers in the limit $R \to \infty$ [25,27], n is the principle quantum number in the same limit:

$$n = n_1 + n_2 + m + 1. \tag{77}$$

We shall mark all the quantities related to this state with the subscript 0. In the limit considered the eigenstate ψ_0 and the corresponding eigenvalue $\varepsilon_0(R)$ of the two-center problem are:

$$\varepsilon_0(R \to \infty) = -\frac{1}{2}; \quad \psi_0 \propto \exp\left(-m_{\mu\mathrm{H}}\, r\right). \tag{78}$$

The atomic wavefunction of μH(1S) with the correct reduced mass is seen to be obtained. This is due to the unit charge in the two-center problem being placed in the center-of-mass of muonic hydrogen. The argument of the exponent in (78) is the distance from this charge to the muon. The eigenvalue of the muon Hamiltonian H_μ (27) tends to the correct dissociation limit (62):

$$m_{\mu\mathrm{H}}\varepsilon_0(R \to \infty) = E_{\mu\mathrm{H}}(1\mathrm{S}). \tag{79}$$

The next step is to be convinced that the potential $U_0(R)$ (74) includes the polarization attraction (19) and no spurious long-range interactions. With this purpose let us consider an asymptotic expansion of $U_0(R)$ in powers of R^{-1}. We confine ourselves to taking into account the terms up to R^{-4} inclusive. The asymptotic expansion of $\varepsilon_0(R)$ is well-known [30]:

$$\varepsilon_0(R) = -\frac{1}{2} - \frac{Z'}{R} - \frac{9Z'^2}{4R^4}. \tag{80}$$

Its substitution into (70) yields:

$$U_0^{(2)}(R) = -m_{\mu\mathrm{H}}\left(\frac{Z'}{R} + \frac{9Z'^2}{4R^4}\right). \tag{81}$$

The next term $U_0^{(3)}(R)$ is obtained by averaging the Coulomb repulsion of the nuclei over the state considered. As the wavefunction ψ_0 is localized near the left center, it is convenient to write the Coulomb repulsion as follows:

$$\frac{Z}{R_{\mathrm{H}Z}} \approx \frac{Z}{R}\left(1 + \sum_{k=1}^{\infty}\frac{\mathcal{M}^{(k)}}{R^k}\right). \tag{82}$$

The multiple moments $\mathcal{M}^{(k)}$ specify the distribution of the charge H with respect to the center-of-mass of the μH atom:

$$\mathcal{M}^{(k)} = r_{\mathrm{H}}^k\, P_k(\cos\theta_{\mathrm{H}}). \tag{83}$$

The vector $\mathbf{r}_{\mathrm{H}}$ connects the center-of-mass with the hydrogen nucleus (Fig. 1):

$$\mathbf{r}_{\mathrm{H}} = -\frac{m_{\mu\mathrm{H}}}{M_{\mathrm{H}}}\,\mathbf{r}. \tag{84}$$

θ_{H} is the angle between the vectors $\mathbf{r}_{\mathrm{H}}$ and $\mathbf{R}$, $P_k(\cos\theta_{\mathrm{H}})$ is the Legendre polynomial. Actually, the moments $\mathcal{M}^{(k)}$ are polynomials in powers of the length of the vector $\mathbf{r}$ and its projection z' on the direction of $\mathbf{R}$. The relations (34) allow one to write the multipole moments in terms of the spheroidal coordinates ξ and η. For example, the dipole moment ($k = 1$) is:

$$\mathcal{M}^{(1)} = -\frac{m_{\mu\mathrm{H}}}{M_{\mathrm{H}}}\,z' = -\frac{R}{2M_{\mathrm{H}}}\,(1 + \xi\,\eta). \tag{85}$$

Averaging the expansion (82) yields:

$$U_0^{(3)}(R) = \frac{Z}{R}\left[1 + \sum_{k=1}^{\infty}\frac{\mathcal{M}_0^{(k)}(R)}{R^k}\right],$$
$$\mathcal{M}_0^{(k)}(R) = \int d\tau\,\psi_0^2(\xi,\eta;R)\,\mathcal{M}^{(k)}. \tag{86}$$

To evaluate the integrals involved here the two-center wavefunction ψ_0 was also expanded in powers of R^{-1} [30,31]. In the approximation considered only the leading contribution of the dipole term $\mathcal{M}_0^{(1)}(R)$ proves to be significant. It is proportional to R^{-2}. Finally, we have:

$$U_0^{(3)}(R) = \frac{Z}{R} - \frac{9ZZ'}{2M_{\mathrm{H}}R^4}. \tag{87}$$

A more complicated problem is to obtain the asymptotic expansion of the nonadiabatic potential $U_0^{(1)}(R)$ which is the diagonal matrix element (69). Its analytical solution needs tedious algebraic calculations. To avoid them we constructed $U_0^{(1)}(R)$ numerically. The terms up to R^{-6} inclusive were taken into account in the asymptotic expansion of the wavefunction ψ_0, and the relevant integrals over the spheroidal coordinates ξ and η were evaluated with the help of Laguerre and Gauss-Legendre quadratures. This way indicated that at large R the potential $U_0^{(1)}(R)$ fell proportionally to R^{-6}:

$$U_0^{(1)}(R) \propto R^{-6}. \tag{88}$$

In our approximation this term is to be omitted. So, the desired asymptotic expansion of the potential $U_0(R)$ is the sum of the expressions (81, 87). The substitution of the value (30) for Z' shows that the terms linear in R^{-1} are exactly cancelled, and only the terms proportional to R^{-4} remain. The result may be written similarly to the polarization attraction (19):

$$U_0(R) = -\frac{\beta_0 Z^2}{2R^4}. \tag{89}$$

The quantity β_0 is:

$$\beta_0 = \beta\, m_{\mu\mathrm{H}}\left(1 + \frac{m_{\mu\mathrm{H}}}{M_{\mathrm{H}}}\right). \tag{90}$$

β is the exact dipolar polarizability (20). It is seen that $\beta_0 \neq \beta$. However, their numerical values are very close. For muonic protium we have:

$$\beta_0 \approx 0.99\,\beta. \tag{91}$$

The one percent polarizability deficit is due to the Coulomb repulsion of the nuclei being nondiagonal in the two-center basis. The corresponding correction to the potential can be easily found within the perturbation theory. It is:

$$\Delta U_0(R) = \sum_{i\neq 0} \frac{\left(U_{0i}^{(3)}\right)^2}{E_0 - E_i}. \qquad (92)$$

The subscript i labels the two-center eigenstates with $m = 0$, E_i are the corresponding eigenvalues of the muon Hamiltonian H_μ (27), $U_{0i}^{(3)}$ are the matrix elements (71). The leading term of this correction is also proportional to R^{-4}. It is contributed by the dipole term in the expansion (82). The two-center wavefunctions and energies are taken in the limit $R \to \infty$, i.e. they coincide with the atomic ones. In this case the sum in (92) is obviously reduced to that involved into the expression (21) for β. We obtain:

$$\Delta U_0(R) = -\frac{\Delta\beta_0\, Z^2}{2R^4}, \qquad (93)$$

where the correction to the polarizability β_0 is:

$$\Delta\beta_0 = \beta \left(\frac{m_{\mu\mathrm{H}}}{M_\mathrm{H}}\right)^2. \qquad (94)$$

The sum of β_0 and $\Delta\beta_0$ is exactly equal to β:

$$\beta_0 + \Delta\beta_0 = \beta. \qquad (95)$$

So, taking into account the only left-center state (76) already provides a good description of the entrance channel at large R: the dissociation limit is correct, no spurious long-range interactions appear (at least in the terms up to R^{-4} inclusive), the polarization attraction is reproduced with one percent accuracy. Below we confine ourselves to this description. For this reason the asymptotic behaviour of the nondiagonal matrix elements coupling different states of the left-center group in the set (65) is not treated here.

2.4.2 The transfer channel

To describe the transfer channel of the reaction (8) within our approach it is necessary to take into account states of the right-center group in the expansion (64). We consider only bound states with $m = 0$. The subscript m is omitted below. The label j additionally marking these states includes their parabolic quantum numbers n_1' and n_2' at infinite R. The principal quantum number is:

$$n' = n_1' + n_2' + 1. \qquad (96)$$

In the limit $R \to \infty$ the states examined do not describe the μZ atom, but correspond to the problem of the muon motion in the field of the fixed Coulomb center Z'. In particular, their wavefunctions do not include the reduced mass of the μZ atom at all. This results from the Jacobi coordinates used being unnatural for the transfer channel. Consequently, the asymptotic expansion of the potential $U_j(R)$ (74) may be expected to involve spurious contributions. The way of constructing this expansion is similar to that explained in Section 2.4.1. Retaining the terms up to R^{-2} inclusive we have [30]:

$$U_j^{(2)}(R) = m_{\mu\mathrm{H}}\, \varepsilon_j(R) - E_{\mu\mathrm{H}}(1\mathrm{S}),$$
$$\varepsilon_j(R) = -\frac{1}{2}\left(\frac{Z'}{n'}\right)^2 - \frac{1}{R} + \frac{3n(n_1' - n_2')}{2Z'R^2}. \qquad (97)$$

To obtain the expansion of the Coulomb repulsion it is convenient to write the internuclear distance as follows:

$$R_{\mathrm{H}Z} = \frac{1}{m_{\mu\mathrm{H}}} \left| \mathbf{R} + \frac{m_{\mu\mathrm{H}}}{M_\mathrm{H}}\, \mathbf{r}_{\mu Z} \right|. \qquad (98)$$

The vector $\mathbf{r}_{\mu Z}$ connects the nucleus Z with the muon (Fig. 1). Its length may be treated to be much less than R because the two-centre wavefunctions are now localized near the right center. The Coulomb repulsion is then expanded in multipole moments related to the right center. Averaging it over the state ψ_j yields:

$$U_j^{(3)}(R) = m_{\mu\mathrm{H}}\, \frac{Z}{R} \left[1 - \frac{3n'(n_1' - n_2')}{2Z'R}\, \frac{m_{\mu\mathrm{H}}}{M_\mathrm{H}}\right]. \qquad (99)$$

The expansion of the nonadiabatic potential $U_j^{(1)}(R)$ is:

$$U_j^{(1)}(R) = \frac{1}{2M_r}\left(\frac{Z'}{n'}\right)^2 + \frac{\alpha_j}{R^2}. \qquad (100)$$

The term linear in R^{-1} is absent here. This result was obtained analytically. The coefficient α_j was evaluated numerically. In treating the muon transfer from protium to neon the following right-center states will be of interest for us:

$$n_1' = m = 0; \quad n_2' = 5, 6 \text{ and } 7. \qquad (101)$$

The principle quantum number n' is respectively equal to 6, 7 and 8. The values of α_j found for these states are given in Table 1.

It is convenient to write the potential $U_j(R)$ in terms of the distance R_t between the nucleus H and the center-of-mass of the μZ atom. At large R it is:

$$R_t = \frac{R}{m_{\mu\mathrm{H}}}. \qquad (102)$$

This relation follows from (98) at $r_{\mu Z} = 0$. Finally, we have:

$$U_j(R) = U_j^{(\infty)} + \frac{(Z-1)}{R_t} - \frac{\mathcal{D}_j}{R_t^2}. \qquad (103)$$

$U_j^{(\infty)}$ is the dissociation limit for the two-center state considered:

$$U_j^{(\infty)} = U_j^{(\infty)}(\mu Z) + \Delta U_j^{(\infty)}. \qquad (104)$$

Here the first term is the correct value of the dissociation limit counted from $E_{\mu\mathrm{H}}(1\mathrm{S})$:

$$U_j^{(\infty)}(\mu Z) = E_{\mu Z}(n') - E_{\mu\mathrm{H}}(1\mathrm{S}). \qquad (105)$$

Table 1. The parameters of the asymptotic expansion (103) for the states (101). The upper values of $U_j^{(\infty)}(\mu Z)$, $\Delta U_j^{(\infty)}$ and $U_j^{(\infty)}$ are given in muon-atom units, the lower ones–in keV. The other values are in muon-atom units.

n_2'	$U_j^{(\infty)}(\mu Z)$ (105)	$\Delta U_j^{(\infty)}$ (108)	$U_j^{(\infty)}$ (104)	α_j (100)	$\mathcal{D}_j(\mu Z)$ (110)	$\Delta\mathcal{D}_j$ (111)	$\mathcal{D}_j$ (109)
5	−0.932	+0.020	−0.912	−0.165	+4.76	−4.61	+0.15
	−5.24	+0.11	−5.13				
6	−0.565	+0.014	−0.551	−0.285	+6.66	−6.38	+0.28
	−3.18	+0.08	−3.10				
7	−0.327	+0.011	−0.316	−0.433	+8.88	−8.44	+0.44
	−1.84	+0.06	−1.78				

$E_{\mu Z}(n')$ is the energy of the μZ atom:

$$E_{\mu Z}(n') = -\frac{m_{\mu Z}}{2}\left(\frac{Z}{n'}\right)^2. \tag{106}$$

$m_{\mu Z}$ is the reduced mass of the atom:

$$m_{\mu Z}^{-1} = M_{\rm Z}^{-1} + 1. \tag{107}$$

The addition $\Delta U_j^{(\infty)}$ is:

$$\Delta U_j^{(\infty)} = -E_{\mu Z}(n')\left(m_{\mu\rm H}^{-1}\, m_{\mu Z}^{-1} - 1\right)^2. \tag{108}$$

As it was expected, the dissociation limit is obtained to be incorrect. It differs from its correct value (105) due to the addition $\Delta U_j^{(\infty)}$. However, this addition is relatively small for the states (101) (Tab. 1). It shifts the dissociation limit by a few percent.

The second term in (103) correctly describes the Coulomb repulsion of the nucleus H and the μZ atom treated as a point charge $(Z-1)$. The term proportional to R_t^{-2} corresponds to the interaction of a dipole moment $\mathcal{D}_j$ with the electric field of H. This moment may be written as follows:

$$\mathcal{D}_j = \mathcal{D}_j(\mu Z) + \Delta\mathcal{D}_j. \tag{109}$$

Here the first term is the component of the dipole moment of the atomic $|n', n_1', n_2', m = 0\rangle$ state along the electric field. It is taken with respect to the center-of-mass of the μZ atom. We have:

$$\mathcal{D}_j(\mu Z) = -\frac{3n'(n_1' - n_2')}{2Z}\left(1 + \frac{Z}{M_Z}\right). \tag{110}$$

The addition $\Delta\mathcal{D}_j$ is:

$$\Delta\mathcal{D}_j = \frac{3}{2}n'(n_1' - n_2')m_{\mu\rm H}\left(m_{\mu\rm H}^{-1}\, m_{\mu Z}^{-1} - 1\right) - \frac{\alpha_j}{m_{\mu\rm H}^2}. \tag{111}$$

The dipole moment $\mathcal{D}_j$ is seen to differ from the correct atomic value (110). Unlike the dissociation limit, the spurious addition $\Delta\mathcal{D}_j$ proves to be very significant for the states (101). In these states the muon is mainly localized between the μZ atom and the H nucleus. Accordingly, the atomic dipole moment $\mathcal{D}_j(\mu Z)$ is positive, and the last term in (103) is an attraction proportional to R_t^{-2}. The addition $\Delta\mathcal{D}_j$ cancels the contribution of the atomic dipole moment in a high degree (Tab. 1). As a result, the attraction becomes appreciably weaker.

Table 2. The matrix elements $U_{ji}^{(s)}(R)$ (the upper values) and $W_{ji}(R)$ (the lower ones) evaluated for the states (101) in the limit $R \to \infty$. The values of the quantum number n_2' given in the left column and the upper row specify the states j and i respectively. The matrix elements are in muon-atom units.

n_2'	5	6	7
5	−0.912	−0.130	+0.0870
	0.0	−0.0592	+0.0376
6	−0.130	−0.551	−0.0984
	+0.0592	0.0	−0.0514
7	+0.0870	−0.0984	−0.316
	−0.0376	+0.0514	0.0

The presented consideration of the asymptotic expansion of the potential $U_j(R)$ was limited to the terms up to R^{-2} inclusive. Actually, we took into account still more terms of higher orders in R^{-1}. The potential was evaluated numerically at large R in the way mentioned in connection with the result (88). The values obtained were approximated by a finite sum of powers of R^{-1}. The coefficients of the lowest powers treated above were taken to be equal to their exact values, the others were fitted with the least squares method.

Let us now discuss the nondiagonal matrix elements coupling different right-center states in the set (65). Again we confine ourselves to bound states with $m = 0$ so that the matrix elements of the Coriolis interaction are not considered. Applying the same method as before we find that as R is increased, the matrix elements $U_{ji}^{(3)}(R)$ and $U_{ji}^{(a)}(R)$ fall proportionally to R^{-2} while $W_{ji}(R)$, $U_{ji}^{(1)}(R)$ and $U_{ji}^{(s)}(R)$ tend to constant values (Tab. 2)[6]. For this reason the corresponding equations in the set (65) remain coupled in the limit $R \to \infty$, and, therefore,

[6] Terms of higher powers of R^{-1} in the asymptotic expansion of the nondiagonal matrix elements are constructed in the way similar to that used for the potentials.

do not describe the muon transfer to any individual states of the μZ atom. Nevertheless, as the muon in a bound right-center state is asymptotically localized near the nucleus Z, a group of such states taken into account in the expansion (64) of the three-body wavefunction somehow describes the migration of the muon from one nucleus to another. In our approach this migration has to be treated as the muon transfer. It is obvious that only the total transfer cross-section may be obtained in this way.

Concerning the nondiagonal matrix elements coupling bound states of different centres, they fall exponentially as R is increased. This is due to the decrease of the overlap of the corresponding two-centre wavefunctions. As a result, the equations describing the entrance and transfer channels are separated at infinite R. Here we use the simplest approximation in which the only left-center state (76) is taken into account. In this case the entrance channel is asymptotically described by the ordinary radial Schrödinger equation with the potential (89):

$$\frac{d^2\chi_0^J}{dR^2} + \left[\kappa^2 - \frac{J(J+1)}{R^2} - 2M_r\,U_0(R)\right]\chi_0^J = 0. \quad (112)$$

χ_0^J is the corresponding radial function. Its superscript P is omitted because the parity is now specified by J: $P = (-1)^J$. The asymptotic momentum of the relative motion in the entrance channel is:

$$\kappa = \sqrt{2M_r\,E_c}. \quad (113)$$

Below we neglect the small difference (91) of the polarizabilities β and β_0, and consider $U_0(R)$ to coincide with the exact polarization potential (19). Subsequent modifications of this potential are related to the electron screening.

2.5 Boundary conditions

As we provided the correct asymptotic description of the entrance channel, the boundary condition for the function χ_0^J at large R is easily formulated:

$$\chi_0^J(R\to\infty) \to \sin(\kappa R - J\pi/2) + Q_0^J \exp i(\kappa R - J\pi/2). \quad (114)$$

The complex amplitude Q_0^J depends on J and κ. The situation in the transfer channel is more complicated. We require that the functions χ_j^J related to this channel involve only outgoing scattered waves at large R. Let us discuss how the corresponding solutions are constructed. Let a block of N_t coupled equations of the form (65) asymptotically describe the transfer channel. Only bound right-center states with $m = 0$ are considered as before. A solution required is sought in the form:

$$\chi_j^J(R) = f_j(R)\,\exp(i\phi(R)). \quad (115)$$

f_j and ϕ are complex functions, ϕ is the same for all j. For brevity we do not mark these functions with J. The substitution of (115) into the set (65) yields a new set of N_t differential equations for f_j and ϕ. The latter is not involved into this set. Only ϕ' and ϕ'' appear there. The prime denotes the differentiation with respect to R. Then each of the matrix elements in the set (65) is approximated by a finite sum of powers of R^{-1} (Sect. 2.4.2). f_j and ϕ' are expanded in an asymptotic series in R^{-1}:

$$f_j(R) = f_j^{(0)} + \frac{f_j^{(1)}}{R} + \frac{f_j^{(2)}}{R^2} + \cdots,$$
$$\phi'(R) = \phi^{(0)} + \frac{\phi^{(1)}}{R} + \frac{\phi^{(2)}}{R^2} + \cdots \quad (116)$$

The function ϕ is obtained by the integration of ϕ' over R:

$$\phi(R) = C_\phi + \phi^{(0)}R + \phi^{(1)}\ln R - \frac{\phi^{(2)}}{R} - \cdots \quad (117)$$

C_ϕ is an arbitrary constant. For example, it may be set equal to $(-J\pi/2)$. Substituting the expansions (116) into the equations for f_j and ϕ and setting the coefficients of the powers of R^{-1} to zero yield an infinite sequence of algebraic equations for the quantities $f_j^{(\gamma)}$ and $\phi^{(\gamma)}$ ($\gamma = 0, 1, ...$). In the lowest order we have:

$$\mathbf{A}\,\mathbf{f}^{(0)} = 0. \quad (118)$$

$\mathbf{f}^{(0)}$ is the column of the N_t coefficients $f_j^{(0)}$, $\mathbf{A}$ is a N_t by N_t Hermitian matrix. Setting its determinant to zero yields an algebraic equation of degree N_t in the unknown $x = (\phi^{(0)})^2$. The coefficients of this equation are real. In general, some of its roots may be negative. Let x_n be such a root. The corresponding values of $\phi^{(0)}$ are purely imaginary: $\phi^{(0)} = \pm i\sqrt{|x_n|}$. It is obvious that the upper sign should be chosen. In this case the functions (115) fall exponentially with increasing R. The transfer channel is actually open provided there is at least one positive root x_p. The value $\phi^{(0)} = +\sqrt{x_p}$ corresponds to an outgoing wave. After the N_t values of $\phi^{(0)}$ have been found, the column $\mathbf{f}^{(0)}$ is constructed for each of them in the standard way.

The next step is to determine the quantity $\phi^{(1)}$ and the column $\mathbf{f}^{(1)}$ of the coefficients $f_j^{(1)}$. The corresponding matrix equation is:

$$\mathbf{A}\,\mathbf{f}^{(1)} = \mathbf{B}^{(0)}. \quad (119)$$

The column $\mathbf{B}^{(0)}$ involves $\phi^{(0)}$ and $\mathbf{f}^{(0)}$ found already. Moreover, $\mathbf{B}^{(0)}$ is linear in $\phi^{(1)}$. As $\det\mathbf{A} = 0$, the set (119) seems to have no solutions. However, this is wrong. Let Δ_j be the determinant obtained from $\det\mathbf{A}$ by the substitution of the column $\mathbf{B}^{(0)}$ for the column corresponding to $f_j^{(1)}$. The standard transformation used in proving Cramer's theorem yields an equivalent set of N_t equations:

$$\det\mathbf{A}\,f_j^{(1)} = \Delta_j. \quad (120)$$

It is not hard to check that $\Delta_j = f_j^{(0)}\mathcal{S}$, where the real and linear in $\phi^{(1)}$ factor $\mathcal{S}$ is independent on j. So, the choice of $\phi^{(1)}$ from the condition $\mathcal{S} = 0$ allows one to set all

the determinants Δ_j equal to zero. As a result, the equations (120) are transformed into the identity $0 = 0$ satisfied at any $f_j^{(1)}$ which remain still undefined. It should be emphasized that the significant fact of the independence of $\mathcal{S}$ on j is due to the asymptotic expansion (100) of the nonadiabatic potential $U_j^{(1)}(R)$ involving no term proportional to R^{-1}. This leads to the R^{-1} term in the potential $U_j(R)$ (103) being the same for all j.

At $\gamma \geq 2$ the column $\mathbf{f}^{(\gamma)}$ of the coefficients $f_j^{(\gamma)}$ obeys the matrix equation:

$$\mathbf{A}\,\mathbf{f}^{(\gamma)} = \mathbf{B}^{(\gamma-1)}. \tag{121}$$

The column $\mathbf{B}^{(\gamma-1)}$ involves the elements of $\mathbf{f}^{(\nu)}$ with $\nu \leq \gamma - 1$. As $\det \mathbf{A} = 0$, this equation has a solution provided

$$\mathbf{B}^{(\gamma-1)} = 0. \tag{122}$$

This condition is rewritten in the form of a set of N_t linear inhomogeneous equations in N_t unknowns $f_j^{(\gamma-1)}$:

$$\mathbf{A}^{(\gamma-1)}\,\mathbf{f}^{(\gamma-1)} = \mathbf{C}^{(\gamma-2)}, \quad (\gamma \geq 2). \tag{123}$$

The matrix $\mathbf{A}^{(\gamma-1)}$ is invertible so that this set has the unique solution. The right side $\mathbf{C}^{(\gamma-2)}$ involves the elements of the columns $\mathbf{f}^{(0)}, ...\mathbf{f}^{(\gamma-2)}$ as well as the quantities $\phi^{(0)}, ...\phi^{(\gamma)}$. Actually, these quantities may be chosen arbitrarily with the exception of $\phi^{(0)}$ and $\phi^{(1)}$ which have been determined. The simplest choice is:

$$\phi^{(\gamma)} = 0, \quad (\gamma \geq 2). \tag{124}$$

In this case the function $\phi(R)$ involves only the main contributions proportional to R and $\ln R$. Another choice of $\phi^{(\gamma)}$ means a redefinition of the coefficients $f_j^{(\gamma)}$. Indeed, the substitution of the expansion (117) into (115) yields factors $\exp\left(-\phi^{(\gamma)}/(\gamma-1)R^{\gamma-1}\right)$ which may be expanded in powers of R^{-1} and, thereby, included in the asymptotic expansion of the function $f_j(R)$. Finally, the set (123) written for $\gamma = 2$ allows one to find $\mathbf{f}^{(1)}$. Then γ is increased by unity, the column $\mathbf{C}^{(1)}$ is constructed, $\mathbf{f}^{(2)}$ is found, etc. In this way we obtain the N_t solutions required. Each of them involves the N_t functions of the form (115). At large R these functions either fall exponentially or present an outgoing wave. For example, if the three states (101) are used to describe the transfer channel in the reaction (3), all the three roots $\phi^{(0)}$ prove to be real, and we have the three outgoing waves. The boundary conditions at $R = 0$ are standard:

$$\chi_j^J(R = 0) = 0. \tag{125}$$

2.6 Cross-sections

The asymptotic radial function (114) may be rewritten as follows:

$$\chi_0^J(R \to \infty) \to \frac{i}{2}\left[\exp\left(-\kappa R + \frac{J\pi}{2}\right) - S_0^J \exp\left(\kappa R - \frac{J\pi}{2}\right)\right]. \tag{126}$$

S_0^J is the diagonal S-matrix element corresponding to the entrance channel:

$$S_0^J = 1 + 2i\,Q_0^J. \tag{127}$$

It may be expressed in terms of a complex phase shift ω_J:

$$S_0^J = \exp(2i\omega_J); \quad \omega_J = \upsilon_J + i\rho_J. \tag{128}$$

As the transfer channel is open, the modulus of S_0^J is less than unity, and the imaginary part ρ_J of the complex phase shift is positive. The real part υ_J may be defined as follows:

$$\upsilon_J = \delta_J + \pi N_J, \tag{129}$$

where $|\delta_J| \leq \pi/2$, and the integer N_J is:

$$N_J = \lim_{R\to\infty}\left[N_0^J(R) - N_B^J(R)\right]. \tag{130}$$

$N_0^J(R)$ and $N_B^J(R)$ are the numbers of zeros of, respectively, the function $\chi_0^J(R)$ and the spherical Bessel function $j_J(\kappa R)$ at the segment $[0, R]$. In the limit $R \to \infty$ both these numbers become infinite, but its difference N_J remains finite. Actually, the product πN_J does not change S_0^J as well as the cross-sections, but its addition is useful because it indicates how strongly the interaction distorts the wave function in the entrance channel.

In our approach the muon transfer cross-section $\sigma_t(1\mathrm{S})$ coincides with the total reaction cross-section. It is a sum of partial transfer cross-sections [29]:

$$\sigma_t(1\mathrm{S}) = \sum_{J=0}^{\infty}\sigma_t^{(J)}; \quad \sigma_t^{(J)} = \frac{\pi}{\kappa^2}(2J+1)\mathcal{P}_J. \tag{131}$$

$\mathcal{P}_J$ is the transfer probability at given E_c and J:

$$\mathcal{P}_J = 1 - \left|S_0^J\right|^2 = 1 - \exp(-4\rho_J). \tag{132}$$

The differential cross-section of the elastic scattering of μH(1S) by the Z atom is:

$$\frac{d\sigma_{el}}{d\Omega} = |f_{el}(\vartheta)|^2. \tag{133}$$

$d\Omega = 2\pi \sin\vartheta d\vartheta$; ϑ is the scattering angle in the center-of-mass frame, $f_{el}(\vartheta)$ is the scattering amplitude:

$$f_{el}(\vartheta) = \sum_{J=0}^{\infty} f_{el}^{(J)}(\vartheta);$$
$$f_{el}^{(J)}(\vartheta) = \frac{i}{2\kappa}(2J+1)(1 - S_0^J)P_J(\cos\vartheta). \tag{134}$$

$P_J(\cos\vartheta)$ is the Legendre polynomial. The total elastic cross-section is:

$$\sigma_{el} = \sum_{J=0}^{\infty}\sigma_{el}^{(J)};$$
$$\sigma_{el}^{(J)} = \frac{2\pi}{\kappa^2}(2J+1)(\cosh 2\rho_J - \cos 2\delta_J)\exp(-2\rho_J). \tag{135}$$

Let us also consider some quantities specifying energy losses of muonic hydrogen in individual elastic collisions with Z atoms. These may be of interest in treating the moderation of muonic hydrogen in a gas mixture. Let $E_{\rm lab}$ and $E_{\rm lab}(1-\epsilon)$ be the energies of μH(1S) before and after an elastic collision. They are specified in the laboratory frame where the Z atoms are assumed to be initially in rest. The relative energy loss ϵ is:

$$\epsilon = \epsilon_m w(\vartheta). \tag{136}$$

ϵ_m is the maximum value of ϵ:

$$\epsilon_m = 4M_r(1+M_{\rm H}+M_Z)^{-1}. \tag{137}$$

For the scattering of muonic protium by neon $\epsilon_m \approx 0.20$. The function $w(\vartheta)$ is:

$$w(\vartheta) = (1-\cos\vartheta)/2. \tag{138}$$

The mean energy loss in an elastic collision is:

$$\langle\epsilon\rangle = \epsilon_m\langle w\rangle, \tag{139}$$

where $\langle w\rangle$ is:

$$\langle w\rangle = \frac{1}{\sigma_{el}}\int d\Omega\,\frac{d\sigma_{el}}{d\Omega}\,w(\vartheta) = \frac{\sigma_d}{2\sigma_{el}}. \tag{140}$$

σ_d is the diffusion cross-section:

$$\sigma_d = \int d\Omega\,\frac{d\sigma_{el}}{d\Omega}\,(1-\cos\vartheta). \tag{141}$$

The spread of energy losses is specified by the mean square deflection of ϵ from $\langle\epsilon\rangle$:

$$\Delta\epsilon = \left[\langle(\epsilon-\langle\epsilon\rangle)^2\rangle\right]^{1/2} = \epsilon_m\Delta w, \tag{142}$$

where Δw is:

$$\Delta w = \left(\langle w^2\rangle - \langle w\rangle^2\right)^{1/2}. \tag{143}$$

$\langle w^2\rangle$ is defined similarly to (140). It is:

$$\langle w^2\rangle = \frac{2\sigma_d-\sigma_v}{4\sigma_{el}}. \tag{144}$$

The cross-section σ_v is:

$$\sigma_v = \int d\Omega\,\frac{d\sigma_{el}}{d\Omega}\,\sin^2\vartheta. \tag{145}$$

Such a cross-section appears in treating the viscosity of gases. σ_d and σ_v may be also expressed as an infinite series in terms of ρ_J and δ_J.

2.7 The integration of coupled equations

Here we discuss the problem of constructing the solution of the set (65) which satisfies the boundary conditions at $R=0$ and $R\to\infty$. Let the set involve N coupled equations. The standard way implies, in particular, that N linearly independent solutions vanishing at $R=0$ are generated by a numerical integration of the equations starting from the origin [32]. These solutions differ in initial slopes of the radial functions at $R=0$. As the equations involve both the first and the second derivatives of these functions, the integration may be carried out with a Runge-Kutta method. However, this procedure was found to be inapplicable in practice. It leads to solutions which are almost linear dependent. This is due to a complicated structure of the potentials $U_j(R)$. Their nonadiabatic parts $U_j^{(1)}(R)$ involve the derivatives of the two-center wavefunctions with respect to R and, therefore, vary abruptly in the quasi-crossing regions. As a result, barriers appear in the potentials. The radial function satisfying the equation with such a potential increases rapidly with R in the subbarrier region. As all the equations are coupled, this increase is transferred to the other functions. Finally, the difference of the initial slopes becomes insignificant, and all the N solutions are obtained to be similar to one another. In this situation it is convenient to take advantage of the multichannel log-derivative method [33]. Let $\mathbf{M}_\chi(R)$ be a N by N matrix, each column of which is a linearly independent real solution vanishing at $R=0$. The upper element of a column is a function $\chi_0^J(R)$ satisfying the equation asymptotically describing the entrance channel. Confining ourselves to bound two-center states with $m=0$ we rewrite the set (65) in the matrix form:

$$\mathbf{M}''_\chi(R)+\mathbf{w}(R)\,\mathbf{M}'_\chi(R)+\left[\mathbf{u}^{(s)}(R)+\mathbf{u}^{(a)}(R)\right]\,\mathbf{M}_\chi(R)=0. \tag{146}$$

The prime denotes the differentiation with respect to R. The elements of the antisymmetric matrices $\mathbf{w}(R)$ and $\mathbf{u}^{(a)}(R)$ are related to the matrix elements involved into the set (65) as follows:

$$[\mathbf{w}(R)]_{ji} = -2M_r\,W_{ji}(R); \quad \left[\mathbf{u}^{(a)}(R)\right]_{ji} = [\mathbf{w}(R)]'_{ji}\,/2. \tag{147}$$

The subscript m is omitted. The nondiagonal elements of the symmetric matrix $\mathbf{u}^{(s)}(R)$ are:

$$\left[\mathbf{u}^{(s)}(R)\right]_{ji} = -2M_r\,U_{ji}^{(s)}(R),\ (j\neq i). \tag{148}$$

Its diagonal elements are:

$$[\mathbf{u}^{(s)}(R)]_{jj} = 2M_r\Big[E_c-U_j(R)\Big] - \frac{J(J+1)}{R^2}. \tag{149}$$

The matrix $\mathbf{M}_\chi(R)$ is invertible everywhere except the origin. This allows one to introduce the so-called log-derivative matrix:

$$\mathbf{Y}(R) = \mathbf{M}'_\chi(R)\,\mathbf{M}_\chi^{-1}(R). \tag{150}$$

The differential equation for $\mathbf{Y}(R)$ follows from (146). It is:

$$\mathbf{Y}'(R)+\mathbf{w}(R)\mathbf{Y}(R)+\mathbf{Y}^2(R)+\mathbf{u}^{(s)}(R)+\mathbf{u}^{(a)}(R)=0. \tag{151}$$

Due to the relation (147) of $\mathbf{w}'(R)$ to $\mathbf{u}^{(a)}(R)$ the latter may be excluded from this equation. With this purpose let us introduce the matrix $\mathbf{X}(R)$:

$$\mathbf{X}(R) = \mathbf{Y}(R) + \frac{1}{2}\mathbf{w}(R). \tag{152}$$

The equation (151) takes the form:

$$\mathbf{X}'(R) + \frac{1}{2}\Big[\mathbf{w}(R)\mathbf{X}(R) - \mathbf{X}(R)\mathbf{w}(R)\Big] + \mathbf{X}^2(R) + \mathbf{u}^{(s)}(R) - \frac{1}{4}\mathbf{w}^2(R) = 0. \tag{153}$$

At the origin $\mathbf{M}_\chi(0) = 0$ while $\mathbf{M}'_\chi(0)$ may be chosen to coincide with the unit matrix. As a result, $\mathbf{Y}(0)$ as well as $\mathbf{X}(0)$ are diagonal matrices with infinite diagonal elements. The equation (153) guarantees that in this case $\mathbf{X}(R)$ is a symmetric matrix everywhere. This equation can be integrated in a way similar to that used in [33]. The integration is terminated in a point R_0 lying in the region where the nondiagonal matrix elements coupling the entrance and transfer channels are negligible. The matrix $\mathbf{Y}(R_0)$ is thus known. The solutions from which the matrix $\mathbf{M}_\chi(R)$ is constructed vanish at $R = 0$, but, generally speaking, they do not obey the boundary conditions at $R \to \infty$. To satisfy them a linear combination of these solutions is taken. The column of the radial functions related to this combination is written as $\mathbf{M}_\chi(R)\mathbf{C}$ where $\mathbf{C}$ is the column of coefficients which are determined by joining in the point R_0 with solutions having the correct asymptotic behaviour. Let us discuss how this join is made. At $R > R_0$ the entrance channel is described by the equation (112). It has two real solutions specified by their behaviour at large R:

$$\chi_0^{(s)}(R \to \infty) \to \sin(\kappa R - J\pi/2);$$
$$\chi_0^{(c)}(R \to \infty) \to \cos(\kappa R - J\pi/2). \tag{154}$$

These solutions are first evaluated in a point R_1 in which the collision energy E_c is much greater than the potential. If the unscreened polarization potential (19) is used, the method described in [32] may be applied. Otherwise the Riccati-Bessel functions may be taken. As a rule $R_1 > R_0$, and an additional numerical integration of the equation (112) should be made to obtain the solutions considered in the point R_0. The $(N-1)$ equations describing the transfer channel at $R > R_0$ remain coupled at $R \to \infty$. Their solutions in the form of outgoing waves are constructed in a point R_2 in the way discussed in Section 2.5. As R_2 is usually greater than R_0, these solutions are continued to R_0 by a numerical integration. The conditions of joining are:

$$\begin{cases} \mathbf{M}_\chi(R_0)\mathbf{C} = \mathbf{S}_\chi(R_0) + \mathbf{E}_\chi(R_0)\mathbf{Q}, \\ \mathbf{M}'_\chi(R_0)\mathbf{C} = \mathbf{S}'_\chi(R_0) + \mathbf{E}'_\chi(R_0)\mathbf{Q}. \end{cases} \tag{155}$$

The upper element of the column $\mathbf{S}_\chi(R)$ is the function $\chi_0^{(s)}(R)$, the other elements are equal to zero. Each column of the N by N matrix $\mathbf{E}_\chi(R)$ is one of the solutions constructed in the form of outgoing waves. In the first column only the upper element does not vanish. It is equal to the sum $\chi_0^{(c)}(R) + i\chi_0^{(s)}(R)$ which tends asymptotically to $\exp i(\kappa R - J\pi/2)$ involved into the boundary condition (114) for the function $\chi_0^J(R)$. Each of the remaining $(N-1)$ columns is a solution associated asymptotically with an outgoing wave in the transfer channel. The upper element of such a column is equal to zero. $\mathbf{Q}$ is the column of unknown complex amplitudes of the outgoing waves. Its upper element is equal to Q_0^J involved into (114). The column $\mathbf{C}$ of unknown complex coefficients is easily excluded from the equations (155). As a result, the matrix equation for $\mathbf{Q}$ is obtained:

$$\big[\mathbf{Y}(R_0)\mathbf{E}_\chi(R_0) - \mathbf{E}'_\chi(R_0)\big]\,\mathbf{Q} = \mathbf{S}'_\chi(R_0) - \mathbf{Y}(R_0)\mathbf{S}_\chi(R_0). \tag{156}$$

Actually, this is a set of N linear inhomogeneous equations for the N complex elements of the column $\mathbf{Q}$. Solving this set we find the amplitude Q_0^J which allows one to evaluate the cross-sections considered in Section 2.6.

3 The muon transfer from protium to neon

3.1 The two-center problem

The first step in a realization of the present method is to choose a finite set of eigenstates of the two-center problem (36) in which the three-body wavefunction is expanded. The charge Z' is now given by (31). We follow the standard view that the muon transfer is mainly due to long-distance quasicrossings of adiabatic terms associated with the entrance and transfer channels. It is known [27] that quasicrossings exist for terms with the same quantum numbers m and n_1. For the state (76) asymptotically describing the entrance channel these quantum numbers are equal to zero. Accordingly, we consider right-center states with $m = n'_1 = 0$. Their wavefunctions $\psi_j(\xi, \eta; R)$ have no nodes in the variable ξ. The subscript j is now the parabolic quantum number n'_2. In solving the two-center problem we used the comparison equation method suggested in [34][7]. The eigenvalues $\varepsilon_j(R)$ obtained in this way for the states with $n'_2 = 5$–9 are shown in Figure 2. The quasicrossings at $R_c \approx 8, 13, 21$ and 37 m.a.u. are clearly seen. The terms involved into a quasicrossing differ in n'_2 by unity. For the states considered the number n_η of nodes of ψ_j in the variable η coincides with n'_2 so that the values of n_η differ by unity also in accordance with the general rule [27]. There are two more long-distance quasicrossings not shown in Figure 2. The first occurs at $R_c \approx 85$ m.a.u. and involves the right-center states with $n'_2 = 9$ and 10. The second is at $R_c \approx 878$ m.a.u. It involves the right-center state with $n'_2 = 10$ and the left-center state (76).

Let us impress that muonic protium in the 1S state and a neon nucleus approach adiabatically from infinity. Until the distance R reaches the outermost quasicrossing point,

[7] Some misprints were found in [34] so the relevant results were rederived.

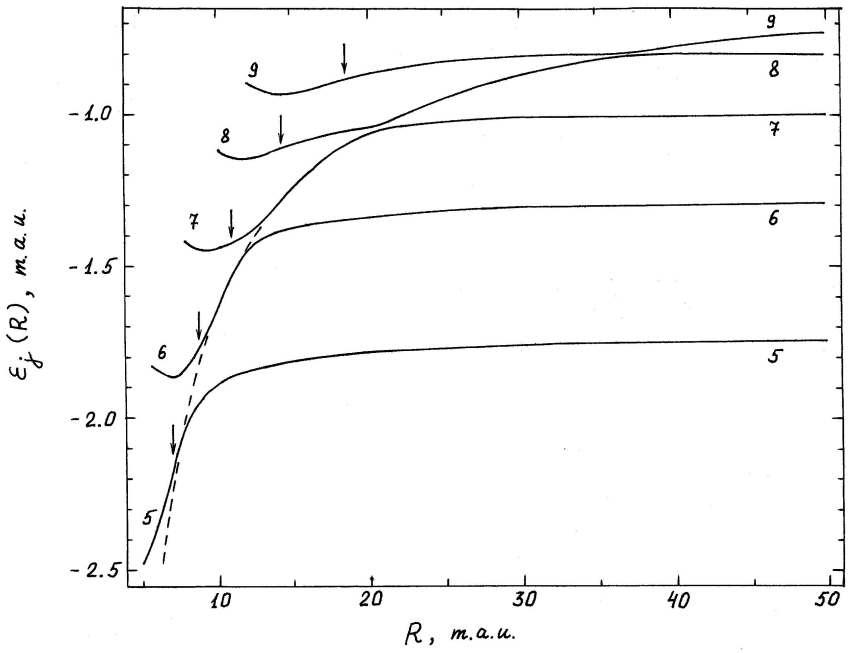

Fig. 2. The eigenvalues $\varepsilon_j(R)$ of the two-center problem vs. the interatomic distance R for the right-center states with the parabolic quantum numbers $m = n_1' = 0$ and $n_2' = 5$–9 (solid curves). $\varepsilon_j(R)$ and R are given in muon-atom units. Any solid curve is marked with a value of n_2'. A vertical arrow indicates the value of R at which the corresponding state crosses the top of the potential barrier separating the Coulomb centers. The dashed curve represents the asymptotic expansion (80) of the eigenvalue $\varepsilon_0(R)$.

the system is described by the wavefunction $\psi_0(\xi, \eta; R)$ correlated to the 1S state at $R \to \infty$ (see (78)). At any finite R this function has eleven zeros, but all of them are located near the center Z' where the function is exponentially small. ψ_0 is mainly localized near the proton where it is the atomic 1S-state wavefunction slightly distorted by the Coulomb field of the charge Z'. The corresponding eigenvalue $\varepsilon_0(R)$ is given by the asymptotic expansion (80). In a very narrow vicinity of the outermost quasicrossing point $R_c \approx 878$ m.a.u. the muon charge distribution in this state changes abruptly. The charge migrates through the potential barrier separating the two Coulomb centers to the right center Z', and ψ_0 becomes exponentially small near the proton. The second state involved into the quasicrossing suffers a similar transformation. On the right of the quasicrossing region its wavefunction ψ_j is localized near the center Z' where it coincides practically with the wavefunction of the corresponding atomic state. On the left ψ_j becomes localized near the proton where it is very close to ψ_0 obtained with the asymptotic expansion in powers of R^{-1} [30,31]. So, after the quasicrossing region has been passed, the right-center state with $n_2' = 10$ actually describes muonic protium in the Coulomb field of neon. The same phenomenon occurs near the other long-distance quasicrossings. For example, at $R < 85$ m.a.u. the state with $n_2' = 10$ becomes localized near the center Z' again while the right-center state with $n_2' = 9$ describes muonic protium and neon. At $R < 37$ m.a.u. the state with $n_2' = 8$ plays this role, etc. Thus, the right-center states with the successively decreasing values of the quantum number n_2' describe muonic protium in the field of neon at R lying between the quasicrossing points. This statement is confirmed by a good agreement of results obtained for these states within the comparison equation method [34] with those found with the asymptotic expansion of ε_0 and ψ_0 in powers of R^{-1}. These results are the eigenvalues ε_j shown in Figure 2 as well as matrix elements involved into the set (65) of coupled equations. Of course, the above statement is wrong in a quasicrossing region where both the states involved are not localized at any center. It should be emphasized that the comparison equation method takes this case into account. As R_c is decreased, the quasicrossings occur closer and closer to the top of the potential barrier separating the Coulomb centers, and the quasicrossing regions become broader (Fig. 2). The quasicrossing at $R_c \approx 8$ m.a.u. occurs almost at the barrier top.

Rigorously speaking, the state (76) describes the entrance channel only on the right of the outermost quasicrossing point $R_c \approx 878$ m.a.u., and all the two-center states considered above should be included into the expansion (64) of the three-body wavefunction. However, the standard view on the muon transfer assumes that only quasicrossings occurring near the barrier top and, thereby, at not too large R are significant. For example, according to [18] the muon transfer from hydrogen to carbon and oxygen is due to quasicrossings at $R_c = 7$–9 m.a.u. A quasicrossing at $R_c \approx 12$ m.a.u. was found to be responsible for the muon transfer to fluorine [35]. The already mentioned results [21] on the muon transfer to neon were obtained in treating quasicrossings at $R_c = 26$–28 m.a.u. In this connection we fully ignore the deep subbarrier

quasicrossings occurring at $R_c \approx 37$, 85 and 878 m.a.u. So, only the two-center states with $n'_2 = 5$–8 are taken into account in the set (65) of coupled equations. As it was explained, on the right of the quasicrossing point $R_c \approx 21$ m.a.u. the state with $n'_2 = 8$ describes muonic protium in the Coulomb field of neon. In this case the muon is mainly localized in a vicinity of the proton where its wavefunction ψ_j coincides well with ψ_0. Accordingly, the potential $U_j(R)$ tends to the polarization attraction (89) with increasing R, and the nondiagonal matrix elements coupling this state with the others fall exponentially. In this sense the state considered is associated with the entrance channel. Actually, this picture becomes wrong near the next quasicrossing point $R_c \approx 37$ m.a.u., but we ignore this effect in accordance with the accepted assumption that the deep subbarrier quasicrossings are insignificant. Thus, on the left of the quasicrossing point $R_c \approx 21$ m.a.u. we have four coupled equations in the set (65). As R increases to the right of this point, the equation for the radial function χ_j^J corresponding to the state with $n'_2 = 8$ is gradually separated from the others and takes the form (112) in which χ_j^J is substituted for χ_0^J. We assume that this equation asymptotically describes the entrance channel. The transfer channel is described by the three coupled equations for the radial functions corresponding to the states with $n'_2 = 5, 6$ and 7.

The subsequent procedure is straightforward. The matrix elements appeared in the coupled equations are evaluated with the formulae of Section 2.3. Here we used the comparison equation method [34] to construct the relevant two-center wavefunctions. At large R the asymptotic expansions of the matrix elements discussed in Section 2.4.2 were applied. The set of the four coupled equations was integrated in the way indicated in Section 2.7. The point R_0 in which the equations associated with the entrance and transfer channels are separated and in which the join (155, 156) is made was taken in the interval 30–35 m.a.u.

3.2 The electron screening

The general treatment presented in Section 2 related to the case in which muonic hydrogen collides with a bare nucleus. Actually, the collision with an atom or molecule occurs so that the presence of the electron shell should be taken into consideration. Generally speaking, the dynamics of the electron shell during the muon transfer is a complicated problem. Indeed, the energy liberated in the muon transfer is of the order of a few keV. It is more than enough for an electron excitation. Accordingly, a more developed treatment is needed in this case. Electron terms in the Coulomb field of the three-body system $\mu\mathrm{H}Z$ should be constructed, and transitions between them should be considered. The simplest approximation is to ignore any excitations and to assume that the electron shell remains in its ground state during the collision. In this case the role of the electron shell is mainly reduced to the screening of the electrostatic interaction of the fragments at large separations. This effect is manifested in both the entrance and transfer channels. For example, in the case of the transfer to neon the incident muonic hydrogen interacts with a neon atom. The assumption that the electron shell is always in its ground state means that the electron state in the transfer channel is similar to the one of the molecule HF, i.e. the ordinary hydrogen atom in the electron 1S state and muonic neon with the electron configuration of fluorine are finally formed. An alternative assumption is that the bare hydrogen nucleus and muonic neon with the electron configuration of the negative ion F^- appear. In any case, as the Jacobi coordinates used in our approach are unnatural for the transfer channel, a way of taking into account the screening is not obvious and needs an additional study. Here we do not concern this question and fully ignore the screening in the transfer channel. This may be partly justified by the relative motion energy in the transfer channel being much greater than the collision energy in the entrance one. For this reason the electron screening in the entrance channel seems to be more significant. It can be easily taken into consideration within our approach. Indeed, on the right of the quasicrossing occurring at $R_c \approx 21$ m.a.u. the nondiagonal matrix elements coupling the entrance and transfer channels fall rapidly, and the polarization attraction $U_0(R)$ (89) appears in the equation asymptotically describing the entrance channel. As it was mentioned at the end of Section 2.4.2 we neglect a percent difference of the polarizabilities β and β_0 and use the exact polarization potential $U_p(R)$ (19) instead of $U_0(R)$. The effect of the electron screening is taken into account by a proper modification of this potential. In this point we followed the method suggested in [36]. The case of neon is favourable because its electron shell is closed. For its description we used analytical one-electron wavefunctions obtained within the Roothan-Hartree-Fock method [37]. The new potential $U_e(R)$ substituted for $U_p(R)$ may be split into three terms:

$$U_e(R) = U_s(R) + U_f(R) + U_w(R). \tag{157}$$

$U_s(R)$ is the screened polarization interaction of muonic hydrogen with neon:

$$U_s(R) = -\frac{\beta Z_a^2(R)}{2R^4}; \quad Z_a(R) = Z - Z_e(R). \tag{158}$$

$Z_e(R)$ is the absolute value of the electron charge inside the sphere of the radius R centered at the neon nucleus. $Z_a(R)$ is the total atomic charge in this sphere. If there are no electrons, $Z_e(R) \equiv 0$ and $U_s(R)$ coincides with the unscreened polarization potential $U_p(R)$.

The term $U_f(R)$ is due to the finite size of muonic hydrogen:

$$U_f(R) = \frac{2\pi}{3} \langle r_{\mu\mathrm{H}}^2 \rangle \rho_e(R). \tag{159}$$

$\langle r_{\mu\mathrm{H}}^2 \rangle$ is the mean-square charge radius of muonic hydrogen in the 1S state. It is taken with respect to the center-of-mass of μH. A trivial calculation yields:

$$\langle r_{\mu\mathrm{H}}^2 \rangle = -\frac{3}{m_{\mu\mathrm{H}}} \left(1 - \frac{1}{M_{\mathrm{H}}}\right). \tag{160}$$

The minus sign is due to the predominating contribution of the negative muon. In the formula (159) the quantity $\rho_e(R)$ is the electron density at the distance R from the neon nucleus. It is normalized as follows:

$$4\pi \int_0^\infty \rho_e(R)\, R^2 dR = Z. \tag{161}$$

One should note that an interaction similar to $U_f(R)$ causes the well-known shift of one-electron S-levels in the field of a finite-size nucleus. In this case the electron density at the nucleus is taken, and the nuclear mean-square charge radius is substituted for $\langle r^2_{\mu\mathrm{H}} \rangle$.

Both the potentials $U_s(R)$ and $U_f(R)$ are attractive and fall exponentially with increasing R. The latter results from an exponential decrease of the charge $Z_a(R)$ and the electron density $\rho_e(R)$. However, as $U_s(R)$ is proportional to the second power of $Z_a(R)$ and, in addition, to R^{-4}, it falls more rapidly. Actually, $U_s(R)$ is significant at distances R less than the electron Bohr radius (≈ 200 m.a.u.). For example, at $R = 30$ m.a.u. $U_s \approx -1.7$ eV, and it exceeds U_f by a factor of twelve. As the electron K-shell of neon has a similar size, the screening effect in U_s is already appreciable. The charge Z_a is about 8.9. At $R \approx 100$ m.a.u. the potentials U_s and U_f become equal. Their sum is about -0.02 eV, i.e. it is of the order of thermal energies. At $R = 200$ m.a.u. U_s is only five percent of U_f. The latter is about -0.002 eV.

The third term $U_w(R)$ in the formula (157) is the potential providing the long-range van der Waals attraction at large R. It appears in the second order of the perturbation theory with respect to the Coulomb interaction of atomic electrons with muonic hydrogen. A calculation of this potential is a complicated problem because it involves a summation over intermediate states of both the electron shell and muonic hydrogen. We confined ourselves to a simple estimation of $U_w(R)$ at large R. In this case the potential may be written in the form of an asymptotic expansion in even powers of R^{-1}:

$$U_w(R) = -\frac{C_6}{R^6} - \frac{C_8}{R^8} - \frac{C_{10}}{R^{10}} - \cdots \tag{162}$$

The leading term proportional to R^{-6} is the van der Waals attraction caused by the interaction of induced dipole moments of neon and muonic hydrogen. The constants of the expansion were evaluated in the completeness approximation. It is based on the assumption that the electron L-shell of neon is mainly deformed in the field of muonic hydrogen while the deformation of the K-shell is less significant. As typical excitation energies of L-electrons are much less than the ones of muonic hydrogen, the sum over intermediate electron states involved into $U_w(R)$ is separated and finally expressed in terms of mean values with respect to the ground state of the electron shell. The constant C_6 obtained in this way is equal to $1.90 \times 10^{+6}$ m.a.u.

In order to elucidate how the electron screening in the entrance channel influences the cross-sections we carried out calculations for the three cases:

(A) the electron screening is fully ignored. The unscreened polarization potential $U_p(R)$ is used in the equation (112);
(B) only the screened polarization potential $U_s(R)$ is substituted for $U_p(R)$. The terms $U_f(R)$ and $U_w(R)$ are not taken into account. Such a way was applied in [15,16];
(C) this is the most realistic case in which the potential $U_e(R)$ is taken to be equal to the sum $U_s(R) + U_f(R)$ on the left of the point R_w where this sum becomes equal to the van der Waals potential $(-C_6/R^6)$. At $R > R_w$ the latter is used as $U_e(R)$. This is the simplest way to provide the correct asymptotic behaviour of the potential. Actually, $R_w \approx 1070$ m.a.u. (about 2.7 Å), and the potential in this point is very small — about 7×10^{-9} eV. So, in our approximation the van der Waals attraction is significant only at extremely low collision energies. We are interested in energies $E_c \geq 10^{-4}$ eV. In this case the van der Waals attraction is manifested in those partial waves for which the outermost classical turning point in the radial equation (112) with the potential $U_e(R)$ lies far on the right of R_w. In particular, it provides the correct dependence of the corresponding phase shifts on E_c and J (Sect. 3.3.2). However, as these phase shifts are small, their contributions to the cross-sections are negligible. So, the main difference of the present case from the case B consists in taking into account the potential $U_f(R)$.

In conclusion, it should be emphasized that our treatment of the electron screening is valid provided the collision energy E_c is less than the lowest electron excitation energy of neon. The latter is about 16.6 eV [38]. For this reason we somewhat arbitrarily placed the upper limit of 15 eV on E_c.

3.3 Results

3.3.1 The muon transfer

The reduced transfer rate $q_t(1\mathrm{S})$ defined in (9) may be written in the form of a partial wave expansion:

$$q_t(1\mathrm{S}) = \sum_{J=0}^{\infty} q_t^{(J)}. \tag{163}$$

The partial transfer rates $q_t^{(J)}$ are expressed in terms of the partial transfer cross-sections (131):

$$q_t^{(J)} = N_{\mathrm{H}}\, v\, \sigma_t^{(J)}. \tag{164}$$

Plots of some partial transfer rates vs. the collision energy E_c are shown in Figure 3. Let us note main features of the curves presented.

At low energies the contribution of the S-wave predominates. The corresponding transfer rate $q_t^{(0)}$ tends to a constant value in the limit $E_c \to 0$. This value depends

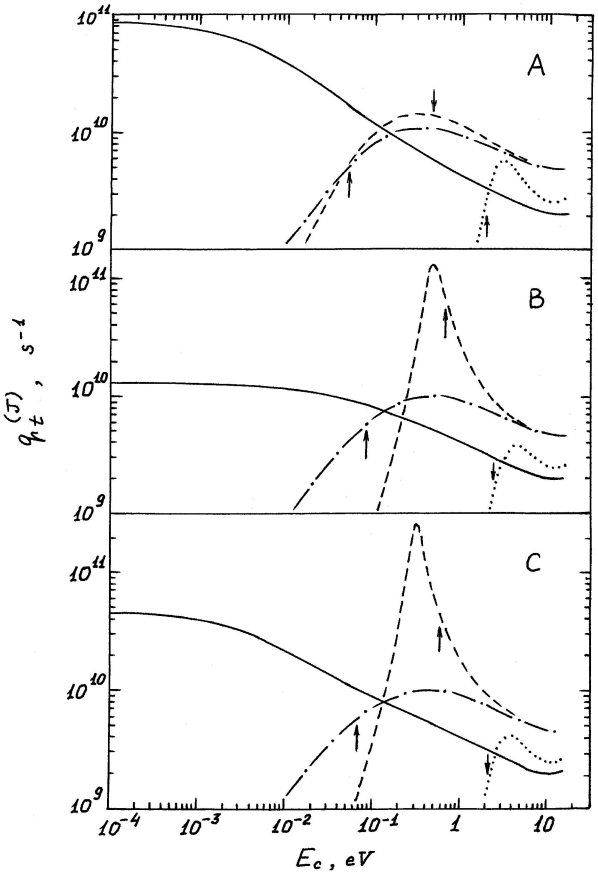

Fig. 3. Some partial transfer rates $q_t^{(J)}$ reduced to the atomic density of liquid hydrogen vs. the collision energy E_c. The three windows correspond to the cases A, B and C. The solid, dash-dot, dashed and dotted curves represent the rates at $J = 0, 1, 2$ and 3 respectively. A vertical arrow indicates the value of E_c at which the state with the given J crosses the top of the hump in the effective potential.

substantially on the way of taking into account the electron screening. It is maximum in the case A in which the screening is fully ignored and the long-range polarization attraction acts in the entrance channel. The electron screening makes this attraction weaker. As a result, in the case B the zero-energy value of $q_t^{(0)}$ falls by a factor of 6.5. The addition of the attraction (159) in the case C increases it by a factor of 3.5.

At low energies $q_t^{(0)}$ is nearly energy independent. This means that the imaginary part ρ_0 of the complex phase shift (128) is linear in v, and the inverse v law is valid for the transfer cross-section in accordance with (11). However, deviations from this law become appreciable at rather small energies. For example, in the case A the value of $q_t^{(0)}$ at $E_c = 2 \times 10^{-3}$ eV is about 70% of that found at $E_c = 10^{-4}$ eV. This contradicts the assumption of [18,21,22] that the S-wave transfer rate remains nearly constant at thermal energies and even above. It should be noted that results on the muon transfer from deuterium to neon obtained in [24] also show that the transfer rate varies at thermal energies. The weakening of the attraction in the entrance channel due to the electron screening makes the energy dependence of $q_t^{(0)}$ smoother. This is especially strongly manifested in the case B in which $q_t^{(0)}$ remains nearly constant right up to thermal energies. The case C is intermediate in this sense.

As the collision energy is increased, the S-wave transfer rate decreases. In the case A the corresponding curve shown in Figure 3 in the log-log scale has a nearly linear segment at $E_c = (0.02{-}0.3)$ eV. In this interval including thermal energies the rate $q_t^{(0)}$ follows the v^{-1} law with a few percent accuracy. The transfer cross-sections falls as E_c^{-1} in accordance with (12). Taking into account the electron screening diminishes the slope of the linear segment. The reason is that the screening decreases the low-energy transfer rate, but it becomes insignificant at $E_c > 1$ eV. In this energy region the difference of the rates $q_t^{(0)}$ calculated for the three cases considered does not exceed a few percent.

Let us come to partial waves with nonzero angular momenta J. The radial Schrödinger equation (112) asymptotically describing the entrance channel involves the effective potential:

$$U_{\text{eff}}(R) = U_e(R) + \frac{J(J+1)}{2M_r R^2}. \qquad (165)$$

At a nonzero J this potential has a hump. The position R_h of its top and its height $U_h = U_{\text{eff}}(R_h)$ are given in Table 3. In accordance with [15] the weakening of the attraction in the potential $U_e(R)$ caused by the electron screening makes the hump higher. At $J \leq 4$ the hump top lies on the right of the outermost quasicrossing point $R_c \approx 21$ m.a.u. which specifies a typical radius of the term interaction region. At low collision energies satisfying the inequality $E_c \ll U_h$ the potential hump prevents the penetration of the corresponding partial wave into the interaction region, and the partial transfer rate $q_t^{(J)}$ is negligible. As E_c goes up to the hump top, $q_t^{(J)}$ increases rapidly and becomes comparable with the S-wave transfer rate at $E_c \sim U_h$. The lowest value of U_h is realized for the P-wave. Depending on the electron screening it varies in the interval 0.052−0.084 eV which joins thermal energies. As a result, the contribution of the P-wave to the muon transfer is already appreciable at these energies. For example, at $E_c = 0.04$ eV ($\approx (3/2)kT$, k is the Boltzmann constant, $T = 300$ K) the ratio of the P- and S-wave transfer rates is equal to 0.22 for the case A and 0.33 for the cases B and C. It is interesting that although the hump height in the case A is least, the P-wave is less significant than in the other cases. This is due to the potential hump being wider in this case — the fact also mentioned in [15]. After the collision energy has become greater than U_h, the P-wave transfer rate passes through a broad maximum and begins to decrease at $E_c > 1$ eV. In this region the electron screening is already insignificant, and the ratio of the P- and S-wave transfer rates varies in the interval 2−2.5.

The situation in the D-wave is especially interesting. In the case A the energy dependence of the partial transfer rate is similar to that found for the P-wave.

Table 3. The position R_h of the top of the effective-potential hump and its height U_h for some J in the cases A–C. In any box the upper value is R_h in m.a.u., the lower one is U_h in eV.

J	A	B	C
1	76.1	62.4	65.6
	0.0519	0.0841	0.0672
2	44.0	39.0	40.5
	0.467	0.641	0.577
3	31.1	28.9	29.5
	1.87	2.32	2.17
4	24.1	23.0	23.2
	5.19	6.05	5.78
5	19.7	19.1	19.2
	11.7	13.0	12.6

The electron screening changes this dependence drastically. The D-wave transfer rate has a resonance peak at $E_c \approx 0.46$ and 0.31 eV in the cases B and C respectively. The reason of its appearance is that the screening modifies the D-wave potential hump in such a way that a quasi-steady state arises somewhat below the hump top. If the collision energy is close to the energy of this state, the D-wave penetrates into the term interaction region, and the muon transfer becomes very effective. For example, in the case B the peak value of the transfer probability $\mathcal{P}_J$ defined in (132) is about 0.53. In the case C it is still greater — about 0.83. As the quasi-steady state lies near the hump top, its effect is manifested right up to collision energies of (1−2) eV. At higher energies the electron screening becomes less significant. It should be also noted that the screening strongly diminishes the D-wave transfer rate compared to the P-wave one at $E_c \leq 0.1$ eV. It is interesting that a peak similar to that discussed above was predicted in the paper [39] in which the muon transfer from protium to oxygen was treated within a semiclassical approach. Taking into account the electron screening in this paper corresponded to our case B, but again the incorrect value of the dipolar polarizability $\beta = 9/2$ m.a.u. was used instead of the correct one (22).

As the collision energy migrates to the region $E_c >$ 1 eV, partial waves with $J \geq 3$ become significant. Main features of the energy dependence of the corresponding partial transfer rates are similar to those found for the P-wave: a rapid increase as E_c goes up to the hump top, a broad maximum above the top and the subsequent fall characterized, in particular, by a gradual decrease of the electron screening effect. The number of partial waves which have to be taken into account in the expansion (163) increases with the collision energy. At the maximum value of $E_c = 15$ eV treated in our calculations the partial waves with $J \leq 6$ are enough to obtain the total transfer rate $q_t(1\mathrm{S})$ with a percent accuracy.

The plot of the total transfer rate $q_t(1\mathrm{S})$ vs. the collision energy is shown in Figure 4. The trend of the curves presented corresponds obviously to the features of the partial transfer rates discussed above. At low energies the S-wave contribution predominates. Accordingly, at $E_c \sim 10^{-4}$ eV the transfer rate is nearly constant. As the energy is increased, the curves obtained for the cases A and C go down while in the case B the rate remains nearly constant. At thermal energies the contribution of the P-wave becomes significant, and the transfer rate begins to increase. As a result, in the cases A and C the transfer rate passes through a minimum lying in the thermal region. At the subsequent energy increase the D-wave becomes involved, and the peak caused by the quasi-steady state appears on the curves calculated for the cases B and C. On the right of this peak the curves pass through one more minimum and at $E_c > 5$ eV begin to go up due to the contribution of waves with $J \geq 3$. The electron screening is not too significant in this region, and all the curves are close to one another.

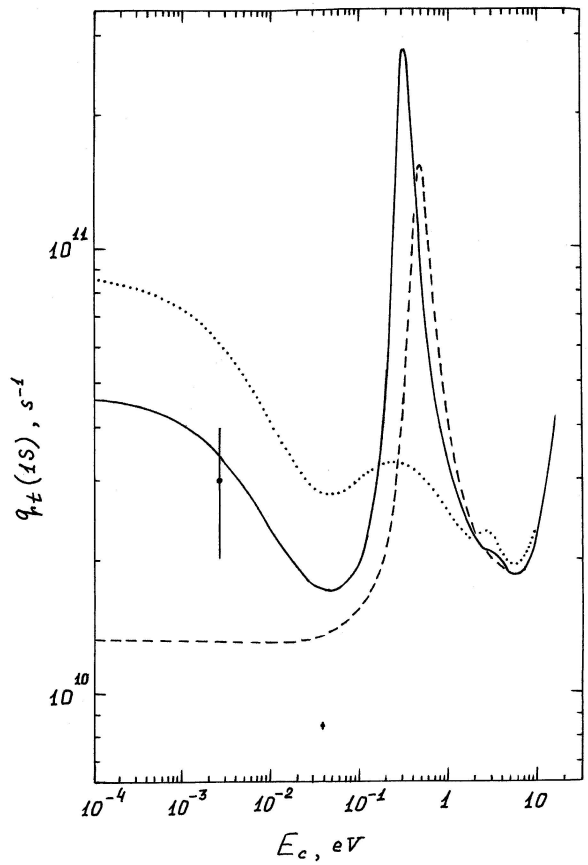

Fig. 4. The total reduced transfer rate $q_t(1\mathrm{S})$ vs. the collision energy E_c. The dotted, dashed and solid curves represent the rate for the cases A, B and C respectively. The experimental values (14) and (4) are attributed to the mean thermal energies $(3/2)kT$ at $T = 20$ and 300 K.

The comparison of the rates presented with the experimental values (14) and (4) attributed in Figure 4 to the mean thermal energies $(3/2)kT$ at $T = 20$ and 300 K shows that the most reasonable agreement is observed in the case C in which the electron screening is taken into account most accurately. Indeed, the transfer rate obtained in this case for the liquid hydrogen temperature

lies within the experimental errors while the rates found in the cases A and B are respectively too large or too low. Concerning room temperatures, the rate calculated in the case C exceeds the experimental value by a factor of two. However, it seems to be very important that the transfer rate has the well pronounced minimum at thermal energies. This result explains (at least qualitatively) why the muon transfer is strongly suppressed at room temperatures. Moreover, the calculation made in the case C correctly reproduces the tendency of decreasing the transfer rate with increasing the temperature in the interval 20−300 K. It is interesting that this tendency is not reproduced in the case B in which the transfer rate is nearly constant right up to thermal energies. For this reason the results obtained in this case seem to be less realistic although in the thermal region the transfer rate is closer to the experimental value. The rates calculated in the case A are too large everywhere. In order to make these conclusions more obvious we averaged the transfer rate $q_t(1S)$ over the Maxwellian distribution and obtained the rate $\lambda_t(1S)$ of the muon transfer from thermalized μp atoms. This quantity is a function of the temperature T and can be directly compared with the experimental values. The corresponding plots are shown in Figure 5. It is seen that as the temperature migrates from the liquid hydrogen value $T = 20$ K to the thermal region, $\lambda_t(1S)$ calculated in the case C falls and passes through a minimum just at $T \approx 300$ K. In this point $\lambda_t(1S) \approx 2 \times 10^{10}$ s^{-1}, i.e. it exceeds the experimental value (4) by a factor of 2.3. The agreement with the experimental rate (14) measured at $T = 20$ K is formally good, but the Maxwellian distribution seems to be a too crude model for liquid hydrogen. Actually, in this case it is better to confine ourselves to the conclusion that at the collision energies typical for liquid hydrogen the transfer rate $q_t(1S)$ is comparable with the experimental value. Of course, in this point we ignore any effects of the surrounding medium on the binary transfer reaction (8). In particular, the distortion of the incoming wave caused by scattering on H_2 molecules is neglected (Sect. 1.3.1). Moreover, we assume that the electron screening effects discussed above are not changed significantly in liquid hydrogen. This assumption seems to be reasonable because a typical screening radius R_s is appreciably less than the mean distance d_{H_2} between H_2 molecules in the liquid. R_s is defined by the condition $|U_e(R_s)| = (3/2)kT$. At $T = 20$ K it is equal to 0.32 and 0.49 Å for the cases B and C respectively. The distance d_{H_2} is of the order of $(N_H/2)^{-1/3} \approx 3.6$ Å. So, the ratio R_s/d_{H_2} is about 0.1.

Coming back to Figure 5 it is also interesting to note that in the case C the rate $\lambda_t(1S)$ increases rapidly at $T > 500$ K. This is a manifestation of the resonance peak in $q_t(1S)$ caused by the quasi-steady state in the D-wave. In the case B the same increase begins at greater temperatures. In the case A the rate $\lambda_t(1S)$ remains nearly constant in the interval 500−1000 K. In conclusion, it should be emphasized that the results presented above clearly indicate the importance of the correct description of the electron screening in the entrance channel. In particular,

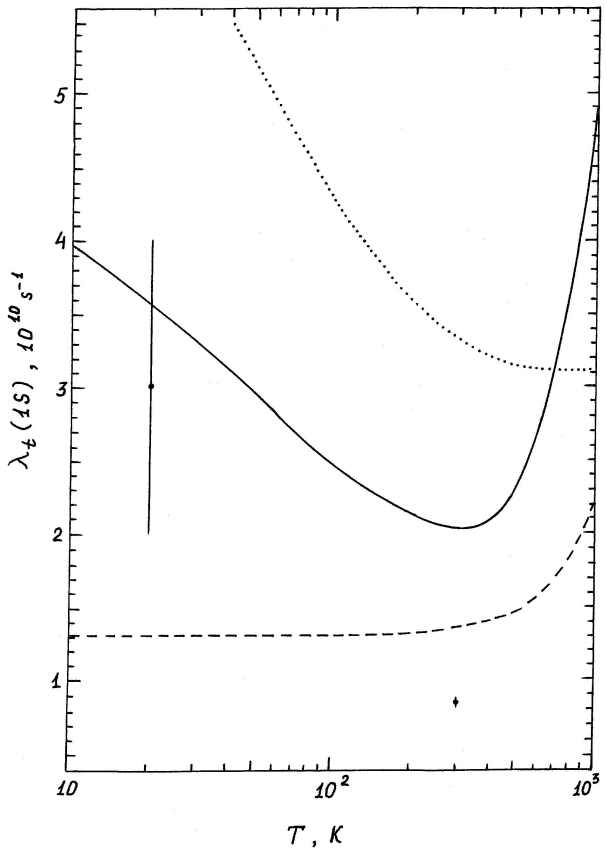

Fig. 5. The reduced rate $\lambda_t(1S)$ of the muon transfer from thermalized μp atoms vs. the temperature T. The notation of the curves is identical to that used in Figure 4. The experimental values correspond to $T = 20$ and 300 K.

taking into account the potential $U_f(R)$ caused by the finite size of muonic hydrogen proves to be very significant.

3.3.2 The elastic scattering

Unlike the partial transfer cross-sections $\sigma_t^{(J)}$ which are determined only by the imaginary parts ρ_J of the complex phase shifts ω_J, the partial elastic cross-sections $\sigma_{el}^{(J)}$ defined in (135) depend also on the real parts. As in our problem it is practically impossible to obtain an explicit form of the radial function $\chi_0^J(R)$ in the term interaction region (Sect. 2.7), we do not consider the integers N_J involved into (129) and confine ourselves to a treatment of the quantities δ_J. Plots of some of them vs. the collision energy are shown in Figure 6. The total elastic cross-section σ_{el} is given in Figure 7. In the same figure we have also plotted the probability of the muon transfer in an individual collision:

$$p_t = \frac{\sigma_t(1S)}{\sigma_t(1S) + \sigma_{el}}. \tag{166}$$

Let us discuss some features of the curves presented.

At low energies we have the S-scattering. The phase shift δ_0 is appreciably greater than ρ_0 and makes the main

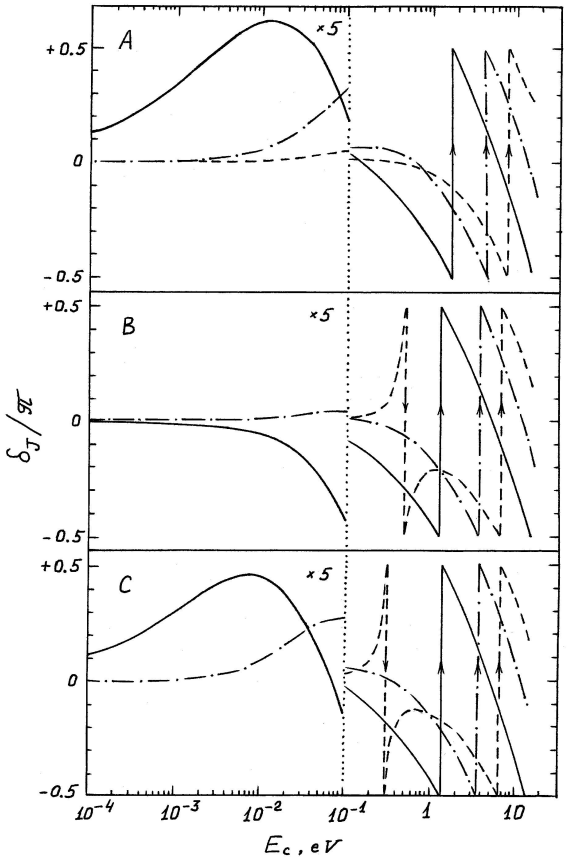

Fig. 6. Some phase shifts δ_J divided by π vs. the collision energy E_c. The three windows correspond to the cases A, B and C. The solid, dash-dot and dashed curves represent the phase shifts at $J = 0, 1$ and 2 respectively. At $E_c < 0.1$ eV the values of (δ_J/π) multiplied by five are given. The vertical dotted line marks the border of this energy region. The vertical arrows indicate jumps of the phase shifts between $(\pm\pi/2)$.

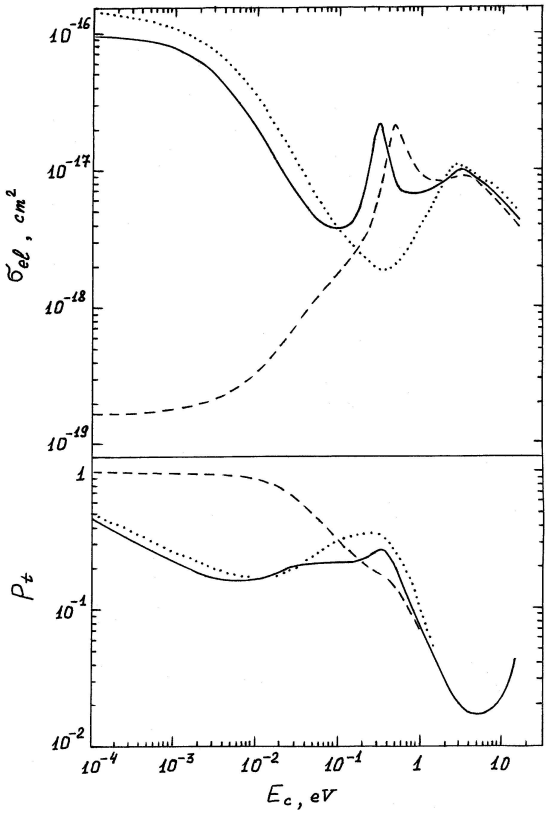

Fig. 7. The total elastic cross-section σ_{el} (the upper window) and the probability p_t of the muon transfer in an individual collision (the lower one) vs. the collision energy E_c. The notation of the curves is identical to that used in Figure 4.

contribution to the elastic cross-section. δ_0 is linear in v so σ_{el} is nearly energy independent unlike the transfer cross-section which is proportional to v^{-1}. In the cases A and C the phase shift δ_0 is positive. The weakening of the external attraction in the case B leads to δ_0 changing its sign and becoming much smaller in the absolute value. As a result, the elastic cross-section falls by three orders of magnitude. It appears, such a behaviour of δ_0 may be attributed to a repulsive effect of the term interaction region.

For the waves with $J \geq 1$ the low-energy phase shifts δ_J are positive and very small. However, they are much greater than the quantities ρ_J so that the scattering of these waves is almost purely elastic. In the cases A and C the phase shifts δ_J agree well with simple results obtained within the Born approximation. For the unscreened polarization attraction (19) this result is [40] (in m.a.u.):

$$\delta_J^B = \frac{\pi\beta\,(M_r Z)^2 E_c}{4\,(J+3/2)\,(J^2-1/4)}. \tag{167}$$

At a fixed J the phase shift is linear in E_c.

In the case C the general Born formula is applied [29]:

$$\delta_J^B = -2\kappa M_r \int_{R_c}^{\infty} U_e(R)\, j_J^2(\kappa R)\, R^2 dR. \tag{168}$$

$j_J(\kappa R)$ is the spherical Bessel function. The lower integration limit is formally equal to zero, but here it is equated to the radius of the term interaction region $R_c = 21$ m.a.u. This is justified by the potential hump suppressing the radial wavefunction in this region. At $E_c \sim 10^{-4}$ eV and $J = 1$ the van der Waals attraction is not yet manifested, and the P-wave phase shifts δ_1 and δ_1^B are proportional to κ^3 in accordance with the general result

$$\delta_J \propto \kappa^{(2J+1)} \tag{169}$$

valid for a short-range potential [29]. As J is increased, the outermost classical turning point in the effective potential $U_{\rm eff}(R)$ migrates into the region $R > R_w$ where the van der Waals attraction acts, and at $J \geq 3$ the phase shifts δ_J follow the Born formula obtained for this attraction [40]:

$$\delta_J^B = \frac{3\pi\, C_6\, M_r^3\, E_c^2}{4\,(J+5/2)\,(J^2-9/4)\,(J^2-1/4)}. \tag{170}$$

At a fixed J the phase shift is now quadratic in E_c.

In the case B the P-wave phase shift δ_1 is a half of the Born one δ_1^B given by the integral (168). This seems to be a manifestation of the repulsive effect of the term interaction region, the contribution of which is fully ignored in the Born integral. As J is increased, this effect disappears, and at $J \geq 3$ the agreement of δ_J and δ_J^B is already good.

As the collision energy is increased, the S-wave phase shift δ_0 calculated for the cases A and C goes up, passes through a maximum and then has a zero at $E_c \approx 0.15$ and 0.075 eV respectively. So, we have a kind of the Ramsauer effect. Unlike the purely elastic scattering, the partial elastic cross-section $\sigma_{el}^{(0)}$ does not vanish at $\delta_0 = 0$ because the quantity ρ_0 remains nonzero. However, $\sigma_{el}^{(0)}$ falls considerably — by three orders of magnitude compared to the energy at which δ_0 is maximum. Although the P-wave cross-section is already appreciable, the Ramsauer effect results in the appearance of a minimum in the total elastic cross-section σ_{el} at $E_c \approx 0.3$ eV (the case A) and 0.1 eV (the case C). In the case B the absolute value of δ_0 as well as σ_{el} increase monotonically with E_c. On the whole, the present behaviour of the S-wave phase shift is similar to that well-known for the elastic scattering of electrons by noble gases [41].

As the collision energy goes up to the top of a potential hump, the contribution of the corresponding partial wave to the elastic cross-section increases rapidly. In the cases B and C the D-wave is especially significant. The presence of the quasi-steady state in this wave leads to the elastic cross-section having a resonant peak similarly to the transfer cross-section. At $E_c = 2$–3 eV there is one more maximum in σ_{el} caused by the collision energy becoming greater than the hump height in the wave with $J = 3$ (Tab. 3). It is interesting that unlike the transfer cross-section, σ_{el} falls at higher energies in spite of the waves with $J = 4$ and 5 becoming involved into the scattering. The electron screening is not very important at such energies.

At some energies there are discontinuities of the curves of δ_J. The phase shift jumps from $(-\pi/2)$ to $(+\pi/2)$. At $J \geq 1$ the energies at which these jumps occur lie above the top of the potential hump in the corresponding partial wave. As the total phase shift υ_J is a continuous function of E_c, each jump is equivalent to the decrease of the integer N_J by unity in accordance with the fact that υ_J tends to zero in the limit $E_c \to \infty$. Another situation is observed near the energy of the D-wave quasi-steady state in the cases B and C. Here the phase shift δ_2 jumps in the opposite direction — from $(+\pi/2)$ to $(-\pi/2)$. This means that the integer N_2 increases by unity as a result of the D-wave penetrating into the term interaction region.

The convergence of the partial wave expansions related to the elastic scattering is determined by the dependence of δ_J on the angular momentum at a fixed collision energy. As J is increased, δ_J tends to the Born values (167–170). In the cases A and C it falls according to a power law — J^{-3} and J^{-5} respectively. For this reason the partial wave expansions involve a much greater number of terms compared to the transfer cross-section. This especially concerns the cross-section of the back scattering. For example, in the case A its evaluation at $E_c = 15$ eV needs taking into account about three hundred waves in order to provide a percent accuracy. However, the use of the Born phase shifts at large J simplifies this problem.

The trend of the curves of the muon transfer probability p_t shown in Figure 7 is determined by the abovementioned features of the transfer and elastic cross-sections. At low collision energies $\sigma_t(1S)$ varies inversely with the relative motion velocity v while σ_{el} is nearly independent on it. Accordingly, $\sigma_t(1S) \gg \sigma_{el}$, and p_t is close to unity. This is especially strongly pronounced in the case B in which σ_{el} is anomalously small. In this case appreciable deviations of p_t from unity are observed only at thermal energies because of a rapid increase of σ_{el} in this region. In the other cases p_t is about 0.5 even at $E_c = 10^{-4}$ eV and remains at the level of a few tenths right up to 0.5 eV. In the case A the Ramsauer effect somewhat increases p_t at E_c around 0.3 eV while in the case C it proves to be insignificant because both the transfer and elastic cross-sections pass through a minimum at $E_c \approx 0.1$ eV. In the same manner the resonant peaks in the cross-sections tell insignificantly on p_t. An interesting feature of the curves presented seems to be the presence of the well pronounced minimum at $E_c \approx 5$ eV. Here p_t drops to 0.017. The reason for which this minimum appears is that the elastic cross-section passes through a maximum at $E_c \approx 3$ eV while the transfer one has a minimum at $E_c \approx 8$ eV.

Let us now come to the quantities $\langle w \rangle$ and Δw which specify energy losses of muonic protium in elastic collisions with neon atoms (Sect. 2.6). Instead of Δw we shall consider the ratio

$$S_w = \frac{\Delta w}{\langle w \rangle} \tag{171}$$

which is a measure of relative deviations of the energy loss from its mean value. Plots of $\langle w \rangle$ and S_w vs. the collision energy are given in Figure 8. The trend of the curves presented is determined by the structure of the angular distribution of the elastic scattering. At low collision energies the S-scattering predominates, and the angular distribution is isotropic in the center-of-mass frame. In this case we have:

$$\sigma_d = \sigma_{el}, \quad \sigma_v = \frac{2}{3}\,\sigma_{el}, \quad \langle w \rangle = \frac{1}{2}, \quad S_w = \frac{1}{\sqrt{3}} \approx 0.577. \tag{172}$$

At greater energies the shape of the curves depends substantially on the way of taking into account the electron screening. For example, in the case B the curve of $\langle w \rangle$ passes through a maximum at thermal energies while in the other cases it has a minimum. To explain this difference let us examine the amplitude of the elastic scattering. At the energies considered it is mainly contributed by the S- and P-waves. This fact together with the inequalities $\rho_J \ll \delta_J \ll 1$ allows one to simplify the formula (134) as follows

$$f_{el}(\vartheta) \approx \kappa^{-1}(\delta_0 + 3\,\delta_1 \cos\vartheta). \tag{173}$$

In the case B the phase shifts δ_0 and δ_1 differ in sign (Fig. 6). As a result, the scattering at angles $\vartheta > (\pi/2)$ is more probable, and the mean energy loss increases compared to the S-scattering. This effect is especially noticed

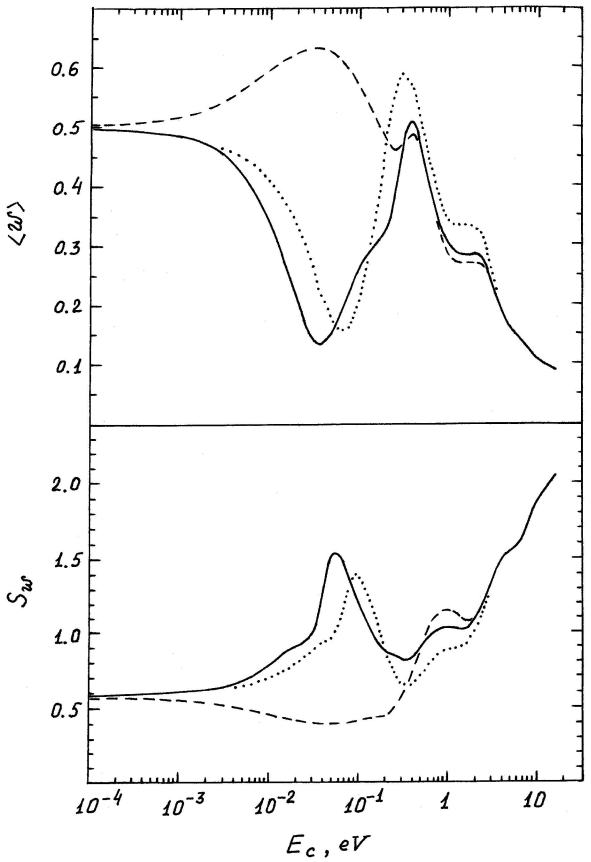

Fig. 8. The mean energy loss $\langle w \rangle$ and the ratio S_w vs. the collision energy E_c. The notation of the curves is identical to that used in Figure 4.

at energies around $E_c \approx 0.04$ eV where the absolute value of the ratio $(3\,\delta_1/\delta_0)$ is maximum — about 0.47. The angular distribution proves to be appreciably peaked backward. For example, the ratio of the differential cross-sections at the angles $\vartheta = \pi$ and 0 is equal to 7.8. In the cases A and C both the phase shifts δ_0 and δ_1 are positive, and the situation is opposite: the scattering at angles $\vartheta < (\pi/2)$ predominates, and the mean energy loss decreases. In these cases the D-wave is also significant. At thermal energies there is a strong cancellation of the contributions of the three waves to the large-angle scattering amplitude. The corresponding differential cross-section is suppressed by 1−2 orders of magnitude compared to the cross-section at $\vartheta = 0$. As a result, $\langle w \rangle$ has a well pronounced minimum in the thermal region. The trend of the curves of S_w is seen to be mainly governed by the behaviour of the denominator $\langle w \rangle$ in the formula (171).

In the interval $E_c = 0.3$–0.5 eV the features of the elastic scattering in the cases B and C are determined by the D-wave quasi-steady state. For the pure D-scattering the amplitude $f_{el}(\vartheta)$ is proportional to the second Legendre polynomial $P_2(\cos\vartheta)$, the differential cross-section is an even function of $\cos\vartheta$, and the quantities σ_d and $\langle w \rangle$ come back to the values (172). In the case C this leads to the appearance of a peak in $\langle w \rangle$. In the case B the same peak is less appreciable. For σ_v and S_w we have:

$$\sigma_v = \frac{10}{21}\,\sigma_{el}, \quad S_w = \sqrt{\frac{11}{21}} \approx 0.724. \tag{174}$$

The quantity $\langle w \rangle$ calculated for the case A is also peaked in the energy interval considered. This is due to the corresponding phase shifts δ_0 and δ_1 differing in sign in this region (see Fig. 6 and the text after the formula (173)).

At the subsequent increase of the collision energy to a few eV the mean energy loss $\langle w \rangle$ decreases rapidly. The mean square deflection Δw changes less regularly. It demonstrates a tendency of decreasing which is slower than the one of $\langle w \rangle$ and accompanied by fluctuations. As a result, the ratio S_w increases. On the whole, the plots of S_w show that Δw is comparable with $\langle w \rangle$ at all the energies considered, i.e. the spread of energy losses is considerable and should be taken into account in, for example, treating the moderation of muonic protium in a hydrogen-neon mixture with a high percentage of neon. Finally, it should be emphasized that similarly to the muon transfer the results on the elastic scattering are very sensitive to the way of taking into account the electron screening in the entrance channel. The effect of the electron screening is significant right up to collision energies of 1−2 eV.

4 Summary

Let us state the most important positions of the present work. The direct muon transfer from protium to neon was theoretically examined in the interval of collision energies from 10^{-4} eV to 15 eV. The elastic scattering of muonic protium by neon was also treated at these energies. A variant of the perturbed stationary states (PSS) method was used. Its basic idea was to provide the correct description of the entrance channel of the transfer reaction at large interatomic distances R. Accordingly, the three-body Hamiltonian was written in the Jacobi coordinates of this channel, and the Coulomb two-center problem was formulated in these coordinates. The expansion of the three-body wavefunction in eigenstates of the two-center problem yielded a set of coupled ordinary differential equations for the radial functions of the relative motion in the entrance and transfer channels. The simplest case was considered in which the entrance channel was described by the only two-center state correlated to the ground state of muonic protium in the separated atoms limit. A good description of the entrance channel at large R has been actually achieved in this way. Namely, the correct dissociation limit was found, the polarization attraction proportional to R^{-4} was obtained in the asymptotic expansion of the interatomic potential in powers of R^{-1}, no spurious long-range interactions of lower powers of R^{-1} appeared, the dipolar polarizability of muonic protium was reproduced with one percent accuracy. Moreover, the electron screening in the entrance channel was easily included into the calculation.

The main simplification made in the present approach was the use of bound eigenstates of the same two-center

problem in describing the transfer channel. Actually, we took into account three σ-states. In the separated atoms limit their parabolic quantum numbers are: $n_1' = 0$, $n_2' = 5, 6$ and 7. Although these states are localized at neon at infinite R, they are not correlated to any individual states of the real μNe atom. As a result, the dissociation limits in the transfer channel were obtained to be incorrect and spurious potentials proportional to R^{-2} appeared. These defects are due to the transfer channel being treated in the Jacobi coordinates of the entrance channel. In this situation the viewpoint had to be adopted that the whole group of the above-mentioned states somehow described the transfer channel. Accordingly, only the total muon transfer rate was evaluated. Moreover, the electron screening in the transfer channel had to be ignored because a way of its taking into account is not yet clear. Nevertheless, the effect of all the above-indicated defects is expected to be not very significant because of large energies of the relative motion in the transfer channel (a few keV). For this reason the present approach seems to be reasonable. Moreover, it appears to be preferable to the standard PSS method [25]. Indeed, the latter provides the asymptotically correct description of neither of the binary channels. This is certainly poor at low collision energies in the entrance channel. In contrast, in the present approach the entrance channel is described well, and all the defects are driven into the transfer channel in which their effect is less significant.

Let us now come to the results on the muon transfer. First of all it is necessary to note that the electron screening in the entrance channel was found to be very important at the collision energies below 1 eV. Its proper treatment allowed one to get a reasonable agreement of the calculated transfer rate with the experimental value measured in a liquid hydrogen-neon mixture at the temperature T about 20 K. It should be emphasized that this statement is valid on the assumption that the additional effects of H_2 molecules on the binary transfer reaction in the liquid are not too significant. The situation at room temperatures proved to be worse: the calculated transfer rate exceeded the experimental one by a factor of two. Nevertheless, two circumstances seem to be very important. Namely, the calculation correctly reproduces the experimentally observed tendency of decreasing the transfer rate with increasing the temperature in the interval 20−300 K, and it predicts the existence of the well pronounced minimum of the transfer rate at $T \approx 300$ K. The latter result corresponds qualitatively to the experimental fact of a strong suppression of the muon transfer at room temperatures. One more interesting prediction is the resonant peak in the transfer rate at collision energies of 0.3−0.5 eV. It is associated with the D-wave quasi-steady state which appears provided the electron screening is taken into account.

Concerning the results on the elastic scattering, they were found to be still more sensitive to the electron screening. This is especially strongly manifested at low collision energies. For example, the total elastic cross-section σ_{el} varies by several orders of magnitude depending on the way in which the screening is taken into account. One should note two effects revealed under the proper treatment of the screening. These are the Ramsauer effect and the D-wave resonance scattering. The former leads to the appearance of the minimum in σ_{el} at the collision energy $E_c \approx 0.1$ eV, the latter results in the cross-section being peaked at $E_c \approx 0.3$ eV. It is interesting that as the similar behaviour is also typical for the transfer cross-section, the probability p_t of the muon transfer in an individual collision proves to be a slowly varying function of the collision energy at $E_c < 0.5$ eV. In this region it is of the order of a few tenths, i.e. the muon transfer competes successfully with the elastic scattering. At greater energies p_t drops rapidly and passes through a minimum at $E_c \approx 5$ eV. Here the elastic scattering predominates. Some interesting features were also found in the energy dependence of the mean energy loss in elastic collisions. Besides the peak associated with the resonance scattering the well pronounced minimum was predicted at thermal energies. In this region there is a strong cancellation of the contributions of the S-, P- and D-waves to the backward scattering amplitude. The differential elastic cross-section proves to be peaked forward and the mean energy loss decreases. This result clearly indicates the importance of taking into account the P- and D-waves even at thermal energies.

This work was supported by the Paul Scherrer Institute (PSI) and by the RFBR grant No. 00–15–96590. I am very grateful to Dr. D. Taqqu who attracted my attention to the present problem. Drs. P. Hauser, K. Kirch, F. Kottmann, R. Pohl, L.M. Simons and Mr. B. Leoni are thanked for their hospitality during my stay at PSI. I am also grateful to Dr. V.D. Efros for fruitful discussions and to Dr. Yu.S. Sayasov who acquainted me with a more detailed version of his paper [21] and clarified some points of his calculations.

References

1. A.I. Akhiezer, V.B. Berestetskii, *Quantum Electrodynamics* (Interscience Publ., N.Y., 1969), Sect. 38.4
2. K. Pachucki, Phys. Rev. A **60**, 3593 (1999); **53**, 2092 (1996)
3. P. Hauser et al., Proposal for an experiment at Paul Scherrer Institute, Villigen, No. R-98-03.1, 1998
4. D. Taqqu et al., Hyperf. Interact. **119**, 311 (1999)
5. K. Kodosky, M. Leon, Nuovo Cim. B **1**, 41 (1971)
6. G. Carboni, G. Fiorentini, Nuovo Cim. B **39**, 281 (1977)
7. T.S. Jensen, V.E. Markushin, preprint PSI-PR-99-32 (Paul Scherrer Institute, Villigen, 1999, `www.psi.ch`)
8. R.O. Mueller, V.W. Hughes, H. Rosenthal, C.S. Wu, Phys. Rev. A **11**, 1175 (1975)
9. J.S. Cohen, J.N. Bardsley, Phys. Rev. A **23**, 46 (1981)
10. F. Kottmann et al., Hyperf. Interact. **119**, 3 (1999)
11. H. Anderhub et al., Phys. Lett. **143**, 65 (1984); **71**, 443 (1977)
12. R. Pohl et al., Hyperf. Interact. **119**, 77 (1999)
13. D. Taqqu, preprint PSI-PR-95-07 (Paul Scherrer Institute, Villigen, 1995, `www.psi.ch`)
14. R. Jacot-Guillarmod, Phys. Rev. A **51**, 2179 (1995)

15. G. Fiorentini, G. Torelli, Nuovo Cim. A **36**, 317 (1976)
16. L. Bracci, G. Fiorentini, Nuovo Cim. A **50**, 373 (1979)
17. A. Adamczak et al., At. Data Nucl. Data Tables **62**, 255 (1996)
18. S.S. Gershtein, Sov. Phys. JETP **16**, 501 (1963)
19. S.S. Gershtein, in *Proceedings of the International Symposium on Muonic Atoms and Molecules, Ascona, 1993*, edited by L.A. Schaler, C. Petitjean (Monte Verita, the Centro Stefano Franscini, Ascona, 1993), p. 169
20. L. Schellenberg, Muon Cat. Fusion **5/6**, 73 (1990/91) and references therein
21. Yu.S. Sayasov, Helv. Phys. Acta **63**, 547 (1990)
22. Yu.S. Sayasov, Phys. Lett. A **159**, 271 (1991)
23. R.A. Sultanov, S.K. Adhikari, Phys. Rev. A **62**, 022509 (2000)
24. R.A. Sultanov, S.K. Adhikari, J. Phys. B **35**, 935 (2002)
25. S.I. Vinitskiĭ, L.I. Ponomarev, Sov. J. Part. Nucl. **13**, 557 (1982)
26. K. Kobayashi, T. Ishihara, N. Toshima, Muon Cat. Fusion **2**, 191 (1988)
27. V.I. Komarov, L.I. Ponomarev, S.Yu. Slavyanov, *Spheroidal and Coulomb Spheroidal Functions* (Science Publ., Moscow, 1976), Chap. 2, Sects. 3.1–3.3, 3.5 (*in Russian*)
28. S.I. Vinitskiĭ, L.I. Ponomarev, Sov. J. Nucl. Phys. **20**, 310 (1974)
29. A.S. Davydov, *Quantum Mechanics*, 2nd edn. (Science, Moscow, 1973), Sects. 43, 44, 109, 118 (*in Russian*)
30. J.D. Power, Phil. Trans. Roy. Soc. Lond. **274**, 663 (1973)
31. R.J. Damburg, R.Kh. Propin, J. Phys. B **1**, 681 (1968)
32. K. Smith, *The Calculation of Atomic Collision Processes* (John Wiley & Sons, N.Y., 1971), Sects. 1.4.4, 2.4.1
33. B.R. Jonson, J. Comput. Phys. **13**, 445 (1973)
34. D.A. Abramov, S.Yu. Ovchinnikov, E.A. Solov'ev, Phys. Rev. A **42**, 6366 (1990)
35. G. Holzwarth, H.J. Pfeiffer, Z. Phys. A **272**, 311 (1975)
36. A.V. Kravtsov, A.I. Mikhailov, N.P. Popov, J. Phys. B **19**, 1323 (1986)
37. E. Clementi, C. Roetti, At. Data Nucl. Data Tables **14**, 177 (1974)
38. A.A. Radzig, B.M. Smirnov, *Parameters of Atoms and Atomic Ions* (Energoatomizdat, Moscow, 1986), Sect. 6.1 (*in Russian*)
39. V.I. Savichev, R. Blümel, Eur. Phys. J. D **21**, 3 (2002)
40. S. Geltman, Phys. Rev. **90**, 808 (1953)
41. H.A. Bethe, R.W. Jackiw, *Intermediate Quantum Mechanics* (W.A. Benjamin Inc., N.Y., 1968), Chap. 14